Electrocoagulation-Based Removal of Polypropylene Microplastics from Water: Process Optimization and Characterization of Fe_3O_4-C Flocs

Thesis submitted

In Partial Fulfilment of The Requirements for the Award of The Degree Of

MASTER OF SCIENCE

IN

CHEMISTRY

Submitted By

Sukhleen Kaur

(3024020018)

Under the supervision of

Dr. Neetu Singh

Professor

Department of Chemical Engineering

Dr. Irshad Mohiuddin

Assistant Professor (Research)

Department of Chemistry & Biochemistry

Department of Chemistry & Biochemistry

Thapar Institute of Engineering and Technology, Patiala-147004

Jan, 2026 - July, 2026

DECLARATION

I, **Ms. Sukhleen Kaur**, hereby declare that the work which is being presented in the thesis entitled **"Electrocoagulation-Based Removal of Polypropylene Microplastics from Water: Process Optimization and Characterization of Fe_3O_4-C Flocs"** is a genuine record of my own work during the period of seven months from January, 2026 to July, 2026 carried out under the supervision of **Dr. Neetu Singh** and **Dr. Irshad Mohiuddin**. This dissertation is submitted in partial fulfilment of the requirements for the award of the degree of **"Master of Science in Chemistry"** in **Department of Chemistry & Biochemistry, Thapar Institute of Engineering and Technology, Patiala**. The information derived from the literature has been duly acknowledged in the text and a list of references is provided. No part of this dissertation is submitted for the reward of any other degree or certificate in this or any other university or institute.

Sukhleen Kaur

(3024020018)

Place: Patiala

Date: 31/07/2026

Dr. Neetu Singh

Professor
Department of Chemical Engineering
TIET, Patiala

Dr. Irshad Mohiuddin

Assistant Professor (Research)
Department of Chemistry & Biochemistry
TIET, Patiala

CERTIFICATE

This is to certify that the dissertation report entitled **"Electrocoagulation-Based Removal of Polypropylene Microplastics from Water: Process Optimization and Characterization of Fe_3O_4-C Flocs"** submitted by **Ms. Sukhleen Kaur (302400018)** in the partial fulfilment of the requirement for the award of the degree of **"Master of Science in Chemistry"** from Department of Chemistry and Biochemistry, Thapar Institute of Engineering and Technology, Patiala, Punjab is an authentic record of student's work carried out during the period of seven months, i.e., from January, 2026 to July, 2026 under our supervision and guidance. This work has not been submitted for the award of any other degree in any other university.

Dr. Neetu Singh

Professor
Department of Chemical Engineering
TIET, Patiala

Dr. Irshad Mohiuddin

Assistant Professor (Research)
Department of Chemistry & Biochemistry
TIET, Patiala

ACKNOWLEDGEMENT

First of all, I want to extend my deepest thanks and gratitude to my supervisors, **Dr. Neetu Singh (Professor)** and **Dr. Irshad Mohiuddin (Assistant Professor- Research), Thapar Institute of Engineering and Technology, Patiala,** for their invaluable guidance, knowledge and patience. Thank you for providing me with the best facilities, which have been important for the completion of this thesis.

I would also like to express my heartfelt gratitude to **Dr. Manmohan Chhibber, Professor and Head of Department of Chemistry and Biochemistry, Thapar Institute of Engineering and Technology, Patiala,** for providing me with this great opportunity and letting me access a variety of the department's resources.

I am deeply grateful to other research group members for their assistance and motivation. I truly appreciate their willingness to share knowledge whenever required. Their friendship and encouragement have made this journey both enjoyable and memorable.

I owe a special thanks to my friends, **Pragnaya Raina** and **Richa Dutta**, who were always there for me and supported me throughout my journey.

I would like to thank my parents and my sister for their unwavering love, encouragement, and support, in every way possible.

Sukhleen Kaur

Place: Patiala **Sukhleen Kaur**

Date: 31/07/2026

LIST OF TABLES

LIST OF FIGURES

LIST OF ABBREVIATIONS

PE	**Polyethylene**
PP	Polypropylene
PS	Polystyrene
PVC	Polyvinyl chloride
UV	Ultraviolet
MPs	Microplastics
EO	Electro-oxidation
PC	Photocatalytic degradation
ROS	Reactive oxygen species
EC	Electrocoagulation
RSM	Response Surface Methodology
ANN	Artificial Neural Network
DC	Direct current
Fe_3O_4/C	Magnetite/Carbon
Fe_3O_4-PP	Magnetite/Polypropylene
NaCl	Sodium chloride
SLS	Sodium Lauryl Sulphate
CCD	Central Composite Design
ANOVA	Analysis of Variance
FTIR	Fourier-transform infrared spectroscopy
XRD	X-ray diffraction
FE-SEM	Field-Emission scanning electron microscopy
EDS	Energy-dispersive X-ray spectroscopy
XPS	X-ray photoelectron spectroscopy
DLS	Dynamic Light Scattering
Fe_3O_4	Magnetite
Fe_2O_3	Hematite

ABSTRACT

Microplastics (MPs) have emerged as a serious threat to humans and aquatic life owing to its persistence and widespread contamination. Among several treatment technologies, electrocoagulation (EC) has garnered significant interest as a reliable, effective and eco-friendly technique for the removal of MPs from water. This study investigates the removal of polypropylene (PP) MPs using EC process with Fe electrodes and examines the valorization of generated EC sludge into functional materials (Fe_3O_4/C) with potential as anode material in Li-ion batteries. The process optimization was done through Central Composite Design under Response Surface Methodology (RSM), evaluating current density, electrolysis time, pH and NaCl concentration as operating variables. An ANN model was developed to predict the process performance and compare its predictive capability with RSM. The EC sludge was carbonized under air and inert conditions and the resultant composites were characterized by FTIR, XRD, FE-SEM, EDS, XPS, DLS and Raman, which proved that carbonized Fe_3O_4/PP flocs under Ar retained Fe_3O_4 with improved structural characteristics. Overall, this study demonstrates EC removing MPs effectively along with generated sludge being converted into value-added materials, thereby, supporting sustainable wastewater treatment and waste to value approach.

Keywords: PP, Electrocoagulation, RSM, ANN and Fe_3O_4-PP flocs

Table of Contents

Chapter 1

Introduction

1.1 Microplastics Production and their Impacts

Plastics are typical synthetic polymers extensively utilized in the industrial and consumer sectors due to their thermal, rheological, mechanical, electrical and optical properties.[1] They are used in packaging of cushion materials, shrink wrap, beverage bottles, kitchenware, cutlery, laundry, buckets, chairs, insulating wires, television housing, sterile syringes, protective masks, clothes, baking and ice trays, ropes, carpets, bumpers, car dashboards, tires and seat covers.[2] However, their accelerating production, persistence, unsustainable use, poor waste management, population increase and urbanisation have resulted in environmental pollution.[3] From the current global trend, almost nine-tenths of total plastic production is mainly composed of polyethylene (PE), polypropylene (PP), polystyrene (PS) and polyvinyl chloride (PVC).[4] 2022 survey shows that plastic production accounted for over 400 million metric tonnes in 2019 and if it still continues, then, by 2060 it will increase to 1.2 billion metric tonnes.[5] A graphical representation of plastics production is depicted in **Fig 1**.

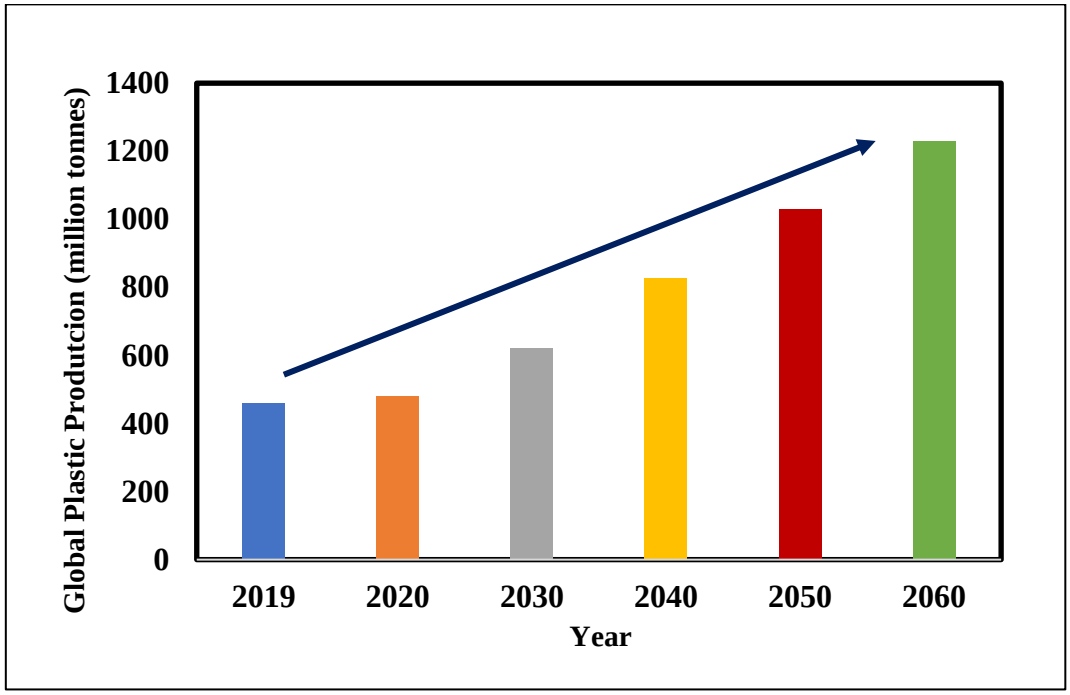

Fig 1: Projected trend of Global plastic production in coming years

Due to slower degradation and long UV-A and UV-C (around 254 nm) exposure to plastics, their presence has led to formation of more minute and harmful particles namely **microplastics**

(MPs).[6] MPs, being one of the most hazardous pollutants in all the three ecosystems (hydrosphere, lithosphere and atmosphere), are tiny fragments of plastics. They vary with particle size of less than 5 µm and are hydrophobic, persistent and have high surface area which aids them in adsorbing various additives.[7] Main sources of MPs include large-sized plastics degradation (packaging bags, bottles), synthetic textile fibres, tire wear, personal care products, marine coatings, city dust, industrial treatments, agriculture and plastic pellets.[8] MPs can be characterized on the basis of their physicochemical properties namely morphology (shape), size and composition. They can be categorized into two types: Primary and Secondary. Primary MPs refer to those which are intentionally produced whereas secondary refers to which are unintentionally produced.[9]

As MPs are omnipresent in marine, freshwater and land ecosystems, they pose a serious threat on the wellbeing of humans, aquatic and terrestrial organisms.[10] Furthermore, their retention in environment finds a way into food chain via accumulation at each trophic level before entering human body.[11] They enter into the body via exposure through inhalation, ingestion and dermal contact. As a result, they cause a detrimental impact on human body through reproductive toxicity[12], growth inhibition[13], weakened nutrient absorption in plants as well as nervous system disorders [14] **(Fig 2)**. Similarly, they affect aquatic life resulting in reduced cell development and lower chlorophyll concentration in phytoplankton [15], immune system deterioration and malfunctioning of gills in fishes [16]. In extreme cases, death may also occur. At present, there are no universally accepted threshold values for MPs in air, water and soil. However, their presence in living organisms generate toxicity effects which are compiled in **Table 1**.

1.2 Remediation Techniques

After the in-depth investigation of MPs impacts, there is dire need for the development of reliable, efficient and eco-friendly methods for degradation and removal of MPs.[17] Recently, various remediation techniques have been invented as a part of wastewater treatment process, mainly categorized as physical, biological and chemical methods. Physical methods, which include filtration and centrifugation, can be effective for separation but are non-destructive for MPs and are energy-intensive.[18] Biological methods, enhanced by microbes, reduce toxicity of MPs but require a way too long time, making it unsuitable for industrial applications.[19] Chemical methods, mainly electro-oxidation, photocatalysis and electrocoagulation, have been found very effective for degradation and removal studies and these have been discussed below.

Table 1: Impacts of MPs on aquatic and terrestrial life:

S. No.	Type of MPs	Organism	Impacts	References
1.	PE, PA, PLA, PBS	*Chlorella vulgaris*	Growth inhibition	[20]
2.	PES, PA, PP, LDPE, PET, PU, PS, PC	*Daucus carota*	All MPs increased plant biomass	[21]
3.	PE	*Zea mays* L.	PE affected expression of antioxidant genes.	[22]
4.	PLA	*Solidago canadensis*	Reduction in plant height, root length and biomass	[23]
5.	HDPE, GPPS	*Brassica chinensis* L.	• GPPS inhibited fresh weight of Chinese cabbage. • Altered leaf soluble sugar and starch concentration.	[24]
6.	HDPE	*Folsomia candida*	Damaged digestive tracts; survival, growth and reproduction suppression	[25]
7.	PVC	*Lactuca sativa* L.	Increased the physiological toxicity to lettuce after getting absorbed and transported in leaves	[8]
8.	PS, PTFE	*Oryza sativa* L.	Highly concentrated MPs reduced • Chlorophyll content • Net rate of photosynthesis MPs induced oxidative burst inside plant tissues	[26]
9.	PP	*Oreochromis niloticus*	Detrimental effects such as changes in organ size and gut microbiota	[27]
10.	PS	*Oryzias melastigma*	MPs exposure adversely affected intestinal microbiota and metabolic homeostasis.	[28]
11.	PVC, LDPE	*Eisenia fetida*	Caused neurological disorders and hindered nutrient absorption	[29]
12.	LDPE	*Lumbricus terrestris*	MPs exposure solely affects their survival	[30]
13.	PP	*Homo sapiens*	Increase in cytotoxicity and oxidative stress	[31]

PE: polyethylene; PA: polyamides; PLA: polylactic acid; PBS: polybutylene succinate; PES: polyethersulfone; PP: polypropylene; LDPE: low density polyethylene; PET: polyethylene terephthalate; PU: polyurethane; PS: polystyrene; PC: polycarbonate; HDPE: high density polyethylene; GPPS: general purpose polystyrene; PVC: polyvinyl chloride; PTFE: polytetrafluoroethylene.

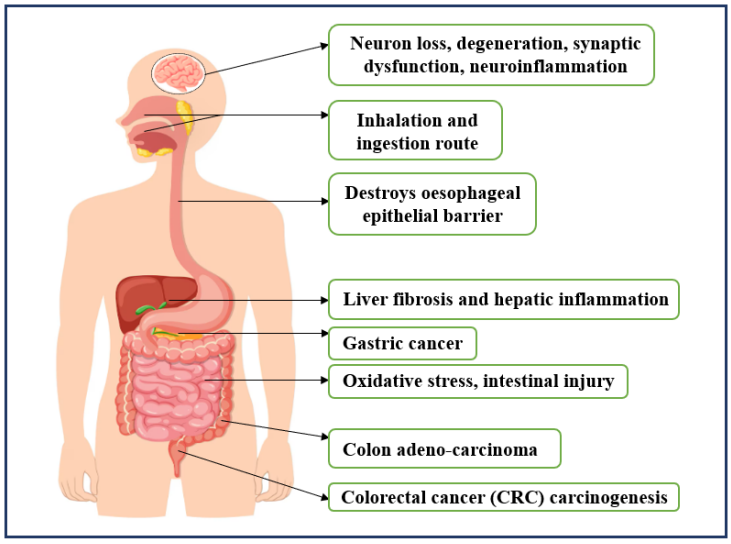

Fig 2: Detrimental effects of MPs on human body

Electro-oxidation, or electrochemical oxidation (EO) is a type of advanced oxidation processes (AOP) which involves oxidation at anode when voltage is applied. It is used for the wastewater treatment and its remediation.[32] The system generally consists of an anode and a cathode connected to a DC power supply and when operating the system with sufficient supporting electrolyte, reactive oxidising species (radicals) are generated, which oxidise and degrades the contaminants (MPs, dyes and drugs). The final products come out as CO_2 and H_2O.[33] It is environment-friendly and can be operated at ambient temperatures and pressure with minimal sludge production. But, EO process requires really high energy consumption, which ultimately hamper achieving high degradation rates.[34] Sometimes, toxic by-products can also be expected when hazardous intermediates like organochlorines are generated.

Photocatalytic degradation is a process of degrading MPs using reactive oxygen species (ROS) generated from semiconductor photocatalysts like TiO_2, ZnO_2 etc upon activation by light.[35] The degradation efficiency generally depends upon light intensity, polymer type, photocatalyst and other reaction conditions.[36] Its major advantages include mineralization, minimal secondary pollution and low chemical consumption.[37] However, its large-scale practical application is quite limited attributing to the slow degradation of persistent polymers, catalyst recovery and dependence on light irradiation.[38]

Electrocoagulation (EC) is a wastewater treatment technique known for removal of heavy metals and pollutants. This method effectively combines coagulation, flotation and electrochemical reactions.[39] Fe (iron) and Al (aluminium) metals are used as sacrificial electrodes as they present outstanding coagulating performance. Its main principle is coagulant

generation via electrochemical oxidation, charge neutralization and electro-flotation facilitating pollutant removal.[40] EC shows several advantages which include high efficiency, less energy consumption and lower sludge volume along with few disadvantages, namely, anode passivation, electrode degradation and formation of metal-laden sludge.[41]

1.3 Electrocoagulation: From MPs Removal to Resource Recovery

As a result, it can be inferred that electrocoagulation is considered a promising approach over electro-oxidation and photocatalytic degradation for MP removal. EC is relatively a very simple, eco-friendly and easy to operate technique which demonstrated higher removal efficiencies (> 90%) for MPs. Unlike conventional coagulation, EC generates in situ coagulants through the dissolution of sacrificial electrodes, thereby, reducing the need for any external additive. It usually requires less energy consumption under optimized conditions. The generated metal-laden sludge can also be valorized further after recovering. The objective of EC process is not only the effective removal of MPs, but also the utilization of waste sludge generated at the end. Earlier, EC sludge was basically disposed of through landfilling or incineration, causing a potential burden environmentally and economically. In contrast, a circular economy approach promotes the recovery and valorization of waste sludge into value-added products, depicting a waste to value approach. The generated flocs, after recovering, can be carbonized or annealed converting into potential materials. Such an approach not only reduces waste production but also enhances the sustainability of electrocoagulation process by converting waste sludge into functional materials with potential energy-storage applications.

1.4 Motivation and Novelty of work

The current study primarily focuses on two objectives- firstly, to provide a sustainable solution for minimizing microplastic pollution in ecosystem and secondly, sustainable valorization of generated waste following a waste to value approach. In this study, Polypropylene (PP) MPs were removed via electrocoagulation process using iron electrodes and the process was optimized through Response Surface Methodology (RSM). While, Artificial Neural Network (ANN) modelling was also employed and comprised the performance comparison of both models. The generated iron oxides- rich flocs as waste were recovered, dried and carbonized under muffle and tubular furnace. The chemical and physical properties of functionalized materials (Fe_3O_4-PP) were investigated using various characterization techniques. This work signifies a sustainable approach converting EC sludge into Fe_3O_4/C materials with potential for energy-storage applications.

Chapter 2

Literature Review

2.1 Polypropylene (PP): Emerging Microplastic Pollutant

Though various polymers are identified as MPs, but, polypropylene (PP) has recently received a substantial attention due its global production and widespread use in packaging (food containers, bottle caps, microwave-safe containers), automotive (bumpers, dashboards, door panels, interior panels), medical (syringes, specimen containers, surgical trays), textiles (ropes, woven sacks, carpets), electrical (cable insulation, capacitor films), agriculture (irrigation pipes, fertilizer bags), laboratory consumables and numerous household items. Owing to its low cost, lightweight property and excellent chemical resistance, it accounts for a significant proportion in global plastic production recent trends.[42] However, their properties result in their persistence in ecosystem, where, they gradually convert into MPs via mechanical abrasion, UV radiation such as UV-A and UV-C (254 nm) and weathering instead of undergoing complete biodegradation.[43] Due to low density (0.8550 g/cm^3- amorphous, 0.946 g/cm^3-crystalline) and hydrophobicity, they can be transported over long distances once released in aquatic environments. Moreover, they also act as carriers that ease toxic contaminants transport inside aquatic food webs, owing to their good adsorption capacity.[44] Rapidly increasing evidence of PP MPs in ecosystem and even human biological samples has raised concerns regarding potential health impacts.[45] Therefore, the development of efficient remediation technologies for PP removal has become the research focus.

2.2 Microplastics (MPs) Remediation Methods

Various physical, biological and chemical techniques for the removal of MPs from water have been investigated. Conventional physical methods, including membrane filtration, sedimentation, flotation, density-separation and magnetic separation, typically remove MPs on the basis of their size, density and structural properties, often showing good removal efficiencies. However, membrane fouling, high operational costs and ineffective removal of minute particles owe notable limitations.[46] Biological treatment methods utilize microorganisms or enzymes to degrade polymers into simpler compounds. Although, being ecofriendly and energy-efficient, its practical application is limited due to the slow degradation rates and its sensitivity in extreme environmental conditions.[47] While, chemical methods, like coagulation-flocculation, advanced oxidation processes, electro-oxidation and photocatalytic

degradation, degrade MPs via chemical reactions. These techniques generally indicate high degradation efficiencies but may need considerable chemical inputs, prolonged reaction times, high energy consumption, restricting their large-scale implementation.[48]

Electro-oxidation (EO) is an advanced electrochemical oxidation technique which aids in degrading MPs through the generation of ROS, particularly hydroxyl radicals ($^{\bullet}OH$) at the anode surface. EO can undergo via direct oxidation (anodic surface) or indirect oxidation through reactive oxidising agents, depending upon the electrode material.[49] Several studies using EO have been demonstrated in **Table 2**. However, the process is often associated with high electrical energy consumption, incomplete mineralization and expensive electrode materials such as boron-doped diamond (BDD), constricting its industrial utilization.[50]

Table 2 Demonstration of MPs degradation efficiencies using EO process

Sr. No.	Type of Microplastics (MPs)	Type of electrode used	Operational parameters	% Removal or degradation efficiency	References
1.	PET	Cathode: Titanium (Ti) Anode: BDD	pH = 6-7, Na_2SO_4 = 0.03M, time = 3 h	90 $\pm$ 3 %	[51]
		Cathode: Titanium (Ti) Anode: BDD	Current = 2 A, Na_2SO_4 = 0.03 M, time = 12 h, MPs conc = 100 mg/L	96 $\pm$ 3 %	[52]
2.	PS	Cathode: Titanium (Ti) Anode: BDD	Current = 2 A, Na_2SO_4 = 0.03 M, time = 10 h, MPs conc = 100 mg/L	81 $\pm$ 3 %	[52]
		Cathode: Titanium (Ti) Anode: Ti/La-Sb-SnO_2	Current density = 46.67 mA/cm^2, electrolyte conc = 0.22 mol/L, pH = 7	28.3 %	[53]
3.	PE	Cathode: Stainless-steel (SS) Anode: Nb/BDD	Current density = 50-100 mA/cm^2, pH = 3-9, V = 100 mL, t = 3 h	Upto 98 % (Py-GC-MS)	[54]
		Cathode: Ti/Pt Anode: Ti/Ru/Ir mixed metal oxide (MMO)	Current Density = 10-30 mA/cm^2, V = 500 mL, MPs conc = 1 g/L, t = 750 h	67 %	[55]
4.	PVC	Cathode: Anode: CeO_2-PbO_2	Current density = 10-60 mA/cm^2, pH = 3-11, V = 150 mL, t = 6 h	Up to 52 %	[56]

Photocatalytic degradation, being an AOP, utilizes photocatalysts like TiO_2 and ZnO under UV light irradiation so as to produce ROS capable of degrading MPs, resulting in mineralization.[57] This technique offers various advantages including utilization of solar energy, but slow degradation kinetics and electron-hole combination and catalyst recovery posing challenges on a large-scale application. **Table 3** summarizes degradation efficiencies using PC process.

Table 3 Representative studies on photocatalytic degradation of MPs

Sr. No.	MPs type	Photocatalyst used	Operating conditions	% Degradation efficiency	References
1.	PE	Nb-doped SnO_2 QDs	200 W Xe lamp, irradiation time = 7 h, MPs conc = 50 mg/ 40 mL	28.9 %	[58]
		g-C_3N_4/TiO_2/WCT-AC	500 W Xe lamp, irradiation time = 200 h, pH = 7.0, MPs conc = 50 mg/ 50 mL	67.58 %	[59]
2.	PP	ZnO NRs coated on glass fiber substrates	120 W tungsten-halogen lamp, irradiation time = 456 h	65 % (reduction in volume)	[60]
		TiO_2@NC	8 W UV-C lamp, Irradiation time = 400 h	5.622 %	[61]
3.	PS	α-Fe_2O_3/g-C_3N_4	35 W Xe lamp, irradiation time = 720 h	3.75 % (0.2 w/v %) 3.45 % (2.0 wt %)	[62]
4.	HDPE	C, N-TiO_2	50 W LED lamp (400-800 nm), catalytic time = 50 h, pH = 3, 0°C	71.77 %	[63]
5.	LDPE	Ag-TiO_2 Fe-Ag-TiO_2 PAM-g-TiO_2	40 W UV lamp (340 nm), Catalytic time = 520 h	13.75 % 14.34 % 39.85 %	[64]

Although EO and PC have represented promising efficiencies for MPs mineralization, their practical application still remains restricted owing to high energy utilization, expensive electrodes or catalysts, prolonged treatment times and limited opportunities for recovery materials.[40] These limitations marks increasing interest in EC which not only favours efficient

MP removal with lower operational costs but also provides recovery and valorization of waste sludge, supporting a sustainable circular economy approach.

Electrocoagulation (EC) is an electrochemical water treatment technology which has gained attention for the removal of dyes [65], heavy metals, oils, MPs and antibiotics.[66] So, it becomes a promising solution making it an attractive choice for industries as it boasts high sustainability and economical operation. The mechanism involves anode passivation using DC current supply. Sacrificial anodes like Iron (Fe) and Aluminium (Al) are used because of their ability of releasing Fe^{2+}/ Fe^{3+} and Al^{3+} ions respectively upon oxidation, thereby, eliminates the need for any external chemical additive. These electrodes intentionally dissolve during EC to generate in-situ coagulant species. The steps in EC process are discussed in the following steps: electro-dissolution of the metal from sacrificial anode (**eq 1**), generation of in situ coagulant species (**eq 2** and **3**), destabilization of suspended particles, interaction of of flocs with colloidal particles and finally, flocs flotation or precipitation (**Fig 3**). The mechanism for EC has been shown in the following equations:

$$Fe(s) \rightarrow Fe^{2+}(aq) + 2e^{-}(aq) \quad (1)$$

$$2H_2O(l) + 2e^{-}(aq) \rightarrow H_2(g) + 2OH^{-}(aq) \quad (2)$$

$$Fe^{2+}(aq) + 2OH^{-}(aq) \rightarrow Fe(OH)_2(s) \quad (3)$$

$$2Fe(OH)_2(s) + \frac{1}{2}O_2(g) \rightarrow 2FeOOH(s) + H_2O(l) \quad (4)$$

$$2FeOOH(s) + Fe(OH)_2(s) \rightarrow Fe_3O_4(s) + 2H_2O(l) \quad (5)$$

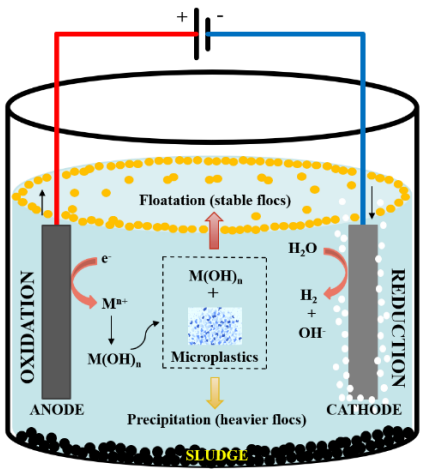

Fig 3: Mechanism for electrocoagulation (EC)

Factors which affect MPs electrocoagulation process include current density, electrolysis time, pH, supporting electrolyte concentration, inter-electrode distance, Microplastic concentration, agitation speed and electrode material. Improper operating conditions may result in excessive energy consumption, electrode passivation and enhanced sludge generation. Therefore, optimization of these parameters is essential to maximize removal efficiency while minimizing energy consumption. Comparison of EC process carried out with different pollutants have been demonstrated in **Table 4**.

Table 4 Comparison of EC studies has been summarized below:

Sr. No.	Pollutant Type	Type of electrode used	Operating conditions	% removal efficiency	Remarks	References
1.	Oily wastewater	Al-Al	CD = 80 A/m^2, pH = 3.6, t = 20 min	78	Optimization = ANN-RSM model Only 1 response (% removal)	[67]
2.	Brilliant Green dye	Fe-SS	CD = 80 A/m^2, initial pH = 5, t = 10 min	98.83	Optimization = ANN-RSM model 2 responses (% removal and energy consumption)	[68]
3.	PP	Fe-Fe	CD = 11.7 A/m^2, pH = 7.7, NaCl conc = 1 g/L	97	Optimization = Only RSM Only 1 response (% removal) No sludge recovery	[69]
4.	Polyester	Fe-Fe	t = 18.38 min, MPs = 200 mg/L, NaCl conc = 363.64 mg/L	100	Full factorial, Box-Behnken No ANN Only 1 response (% removal)	[70]
5.	PP	Fe-Fe	CD = 64.084 A/m^2, t = 79 min, NaCl conc = 2.5 g/L, pH = 7	90.33	Optimization = ANN-RSM model 2 responses (% removal and energy consumption)	This study

CD = Current density

The generated sludge is generally considered a waste which requires disposal, although EC efficiently removes MPs. Recently, researchers proposed valorization of waste sludge into value-added materials. Iron oxide-rich EC sludge possess a notable potential as a precursor for iron oxide/carbon composites, providing opportunities for energy storage applications. Thus, Integrating EC process optimization along with Iron oxide-rich sludge valorization presents an encouraging and sustainable strategy for wastewater treatment and resource recovery.

2.3 Research Gaps

Several research gaps still prevail even after significant progress in electrocoagulation for MPs removal which are discussed below:

- Most studies emphasize only removal efficiency without optimizing energy consumption simultaneously.
- Application of integrated RSM-ANN for modelling is still limited.
- Sludge after EC process is still considered as a waste instead of being recovered.
- The potential application of carbonized EC sludge has received very limited attention as an energy-storage material.

2.4 Objectives

The Objectives of the present study include:

- Removal of PP MPs from water using electrocoagulation.
- Optimization of EC process through RSM-ANN model.
- Synthesis of Fe_3O_4/C composites from EC sludge through carbonization.

The first part deals with mitigating MPs pollution while the second part focuses on utilization of waste into functional materials to be used for energy storage applications.

Chapter 3

Materials and Methodology

3.1 Workflow of current study

The summarized version of current work is represented in **Fig 4**.

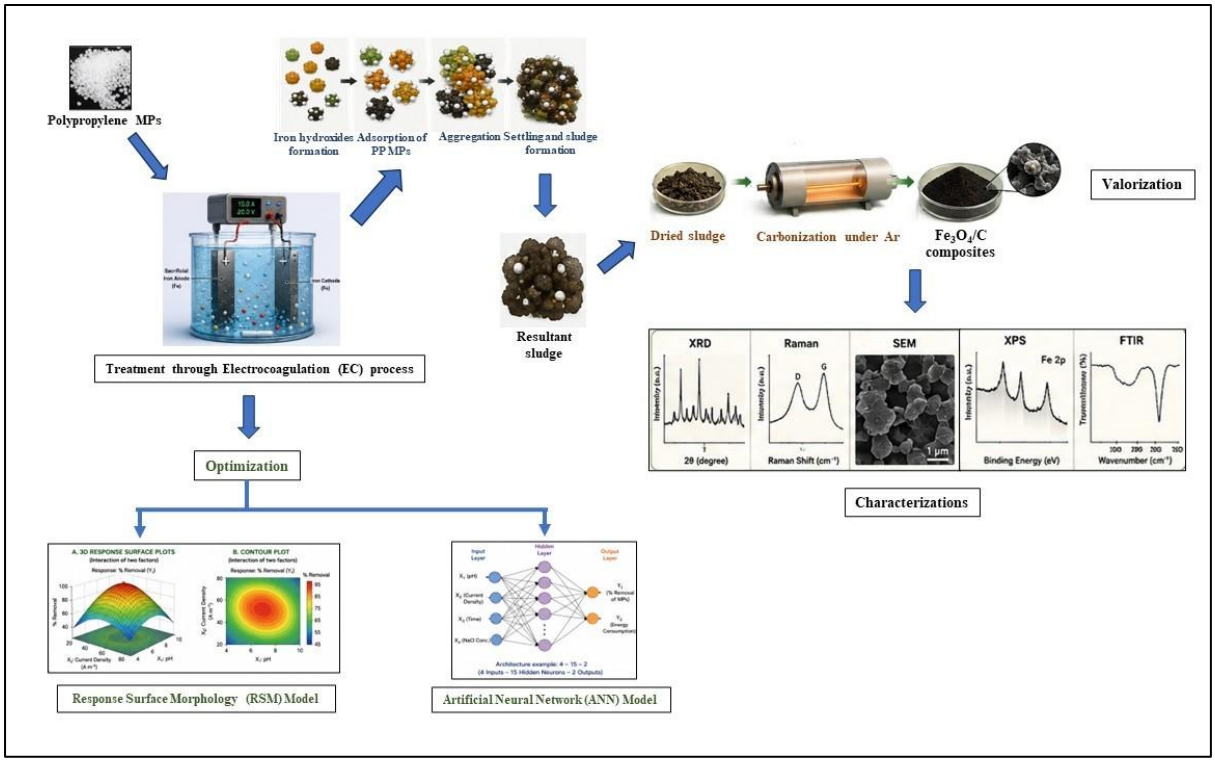

Fig 4: Workflow of current research

3.2 Materials

The materials used in this study include Polypropylene microplastics (PP-MPs, SC201LV) sized between 150-180 µm were obtained from Veera Polypacks Pvt. Ltd., Ludhiana, India. Iron plates (13.6 cm × 4 cm × 0.2 cm) were sourced from Aarvi Energy^{TM}, Nashik, Maharashtra. All chemicals, including sodium chloride (NaCl, ≥ 99.5 %, LOBA Chemie), sodium lauryl sulphate (SLS, ≥ 99 %, LOBA Chemie), pH meter (Aquasol Digital pen type) and Grade 1 Whatman filter paper were purchased from local suppliers. Distilled water was used from the department only. Sand paper was obtained from a paint shop nearby. Muffle and tubular furnace were utilized from department only.

3.3 Methods

3.3.1 Solution Preparation

In this study, PP was selected for investigation of the removal process due to its widespread use in the plastic industry. PP pellets were grinded first into particle size of below 250 µm and then, these powders were sieved through the mesh sizes: 180 µm and 150 µm using sieve shaker. MPs, accumulated between 180 -150 µm size sieves, were taken into account. Synthetic wastewater was prepared using 1 L of distilled water. Sodium Chloride (NaCl) was added in varying amounts to change the solution conductivity. 1N NaOH and 1N HCl solutions were used to maintain the initial pH of the solution. Due to the hydrophobicity of PP MPs and their tendency to float on water (lower density), SLS was added as a surfactant to ensure uniform suspension. SLS concentration at 20 mg/L while PP-MPs concentration at 75 mg/L were maintained in all the experiments.

3.3.2 Experimental set-up

The electrochemical MPs removal was carried out in a customized beaker (1 L), made up of plexiglass, along with a tap around 2 cm above the bottom of it. The beaker was of 14 cm height with diameter of 7 cm. The lid over the beaker had six slots each with 14 mm length and 2 mm width in which iron electrodes were held. A monopolar parallel electrode configuration was employed, in which two iron anodes were connected to the positive terminal and the two iron cathodes were connected to the negative terminal of the DC power supply (12-24 Volts and 0-12 A, Rainbow) to provide the electrical current to the system. The electrode spacing was fixed at 1 cm and each anode had an immersed projected area of 40 cm^2; therefore, a total anodic projected area of 80 cm^2 was adopted for determining the applied current corresponding to the selected current density levels during EC experiments. During all the runs, volume of distilled water (1 L), SLS concentration (20 mg), MPs concentration (75 mg), inter-electrode gap (1 cm) and stirring speed were kept constant. The mixture was agitated by a magnetic stirrer (at 500 rpm with the help of magnetic bead. During each reaction, the current and voltage readings for the energy consumption calculations were recorded when the voltage was stable. After each EC run, the beaker was allowed to stand for some time so that heavier flocs settle down as sludge. After settling, the residual liquid was collected in another beaker and then, was filtered using filter paper. This filter paper was dried in the oven at 60°C for 3 hrs. While the sludge, collected in the beaker, was also filtered using a new filter paper and it was also kept in oven until it is fully dried. Before each EC run, the iron electrodes were rubbed with the sandpaper

so as to remove the deposited oxide layers on the surface. This was done in order to prevent surface oxidation and maintaining consistency in electrochemical performance during all experiments.

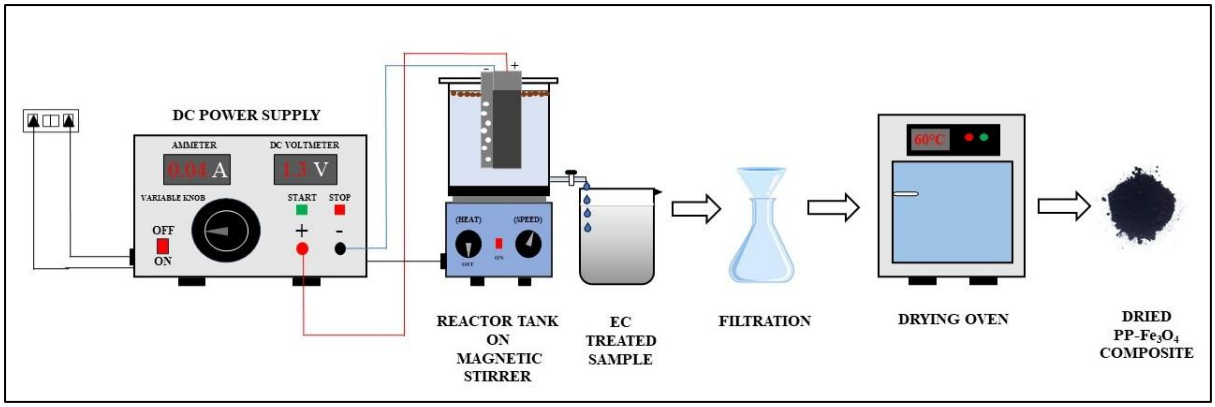

Fig 5: Diagrammatic representation of Electrocoagulation setup

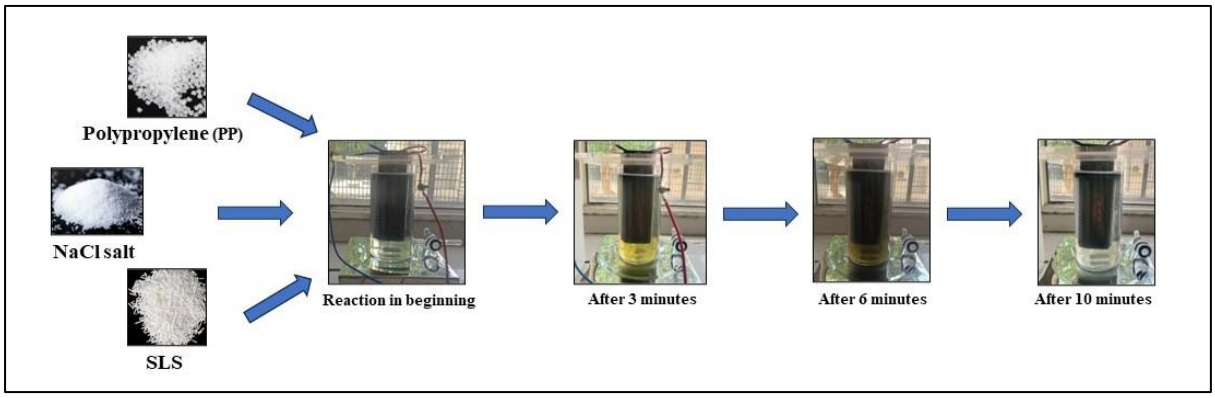

Fig 6: Colour change observed during EC process

3.3.3 Experimental Design

3.3.3.1 Response Surface Methodology (RSM)

Response Surface Methodology (RSM) is a static analytical technique which represents the relationship between dependent and independent variables by taking more than one or more response to determine experimental studies. This contains variations within given ranges for the optimization of different selected parameters. Traditional optimization focuses on only one parameter at a particular time which results in a cumbersome and costly process. This method is known for reducing cost and saving time by reducing the number of experimental runs. Within this method, there are different investigational design models, such as, pentagonal, Central Composite Designs (CCD), hexagonal, Box-Behnken Designs (BDD), Doehlert Matrix (DM) and so on. In RSM, designing is mainly done in three steps: (a) study the interaction

between dependent and independent variables, (b) then selecting the suitable model from RSM design expert software, (c) finally, implementation of experiments and calculating valuable results.

3.3.3.2 Design of experiments and Optimization

In the current study, the Central Composite Design (CCD) was employed in the RSM using Design Expert 13 software. Experiments for electrocoagulation process determining % removal and energy consumption were designed using CCD/RSM. Precision is a significant key of CCD technique. In order to increase the model reliability, it is mandatory to include two additional points that lie outside the initial and final boundaries of a particular interval. As a result, this method allows a more thorough investigation of the response surface. The design is generally conducted at five unique levels (-2, -1, 0, 1, 2). The mentioned five levels enable a thorough understanding of how the variable influences the results both within and outside the specific range. Therefore, this model helps in analysis of the interaction between parameters on responses, ultimately enhancing the accuracy and precision of the experimental results. Additionally, it involves six repetitions at central points for modulation and optimization.

The process variables involved were pH (4-10), current density (20-80 A/m^2), Electrolysis time (10-90 min) and NaCl concentration (0.5- 2.5 g/L). Table presents the range of the variables of the design model. % removal (X_1) and energy consumption (X_2) were selected as responses.

Table 5 Range of Variables and Levels of the Design Model.

		Range of actual and coded variables				
Factors	Variables	(-2)	(-1)	(0)	(+1)	(+2)
A	pH	4.0	5.5	7.0	8.5	10
B	Current density (A/m^2)	20	35	50	65	80
C	Electrolysis time (min)	10	30	50	70	90
D	NaCl concentration (g/L)	0.5	1.0	1.5	2.0	2.5

The quadratic model was applied for the experimental data fittings, analysis and optimization of parameters; its **equation 6** is given below.

$$X = \psi_0 + \sum_{i=1}^{k} \psi_i x_i + \sum_{i=1}^{k} \psi_{ii} x_i^2 + \sum\sum_{i<j} \psi_{ij} x_i x_j + D_r \qquad (6)$$

Where, ψ_0 = constant-coefficient; ψ_i , ψ_{ii} , ψ_{ij} = Interaction coefficients; x_i and x_j = variables; D_r = error. There is a total of k independent parameters.

Analysis of Variance (ANOVA) was used for parameter interaction analysis and the relationship between the answers and the influential factors. Further, the efficacy of the quadratic model was assessed by adequate precision, studentized residuals plots, normal probability plots, coefficient of determination (R^2), predicted R^2, adjusted R^2, F- and P- values. A multi-response optimization tool was employed for the optimization of the two responses, X_1 and X_2 with the help of desirability function of RSM. This tool optimizes the responses based on the set target. While, the desirability function converts the individual desirability (d_i: 0-1) of the responses, X_1 and X_2, into one single desirability value of the system.

3.3.3.3 Data Analysis

In the current study, a total of 30 experiments in the batch mode were performed as designed by CCD/RSM, and % removal (X_1) and energy consumption (X_2) were measured. After the filtration process, the filter paper with PP MPs were dried in oven at 60°C for 3 hrs and subsequently weighed using a weighing balance. The removal efficiency each time was calculated based on the change in filter paper's weight **(Eq 7)**. For accurate reading, one filter paper was dried under same conditions to note down its reading. All the measurements were repeated twice and the average values were reported.

$$\%\ Removal\ (X_1) = \frac{(C_0 - C_f)}{C_0} \times 100 \qquad (7)$$

Where, C_0 = Initial PP microplastic concentration (mg/L); C_f = Final concentration (mg/L)

Furthermore, energy consumption (kWh/m^3) was calculated as:

$$Energy\ consumption\ (E), (X_2) = \frac{V \times I \times t}{1000 \times V_s} \qquad (8)$$

Where, V = cell voltage (in volt); I = current (A); t = electrolysis time (hours); V_s = Volume of solution (m^3) and E in kWh/m^3.

The pH, current, voltage and conductivity were checked thoroughly during all the experiments. With the progress of the electrocoagulation process, the solution became more turbid, attributed to the formation of flocs. After settling for some time, the residual liquid was more transparent in comparison to the initial one. The sludge containing Fe_3O_4-PP flocs, which got settled at the bottom, was separated using external magnet and recovered after drying it at 60°C for 24 hrs. These flocs were stored and further used for characterization.

3.3.3.4 Artificial Neural Network (ANN) modelling

In this study, multilayer perception (MLP) is used which is made up of layers of neurons. The first layer of neurons symbolizes the independent variable inputs. From ANN, the relative effect of each input neuron can be determined along with the intricate interconnections on the observed outcome. Here, the MLP contains four input neurons that indicate pH, current density, electrolysis time and NaCl concentration, single hidden layer of neurons and two output neurons namely % removal and energy consumption. Number of data sets were fed, out of which 70% of the datasets were employed for training, while remaining 30% was further divided into testing and validation. L-BFGS (Limited-memory Broyden-Fletcher-Goldfarb-Shanno) was used as training algorithm for ANN model. This algorithm generally works good for small datasets as it is second-order optimization method and converge very fast without oscillation producing smooth loss curves.

3.4 Carbonization

The Fe_3O_4-PP flocs were carbonized under inert (Argon atmosphere) and air conditions. The sample was carbonized at 500°C for 2 hrs under air in muffle furnace. Another sample of flocs was annealed at 500°C for 2 hrs at the ramping rate of 5°C/ min. After carbonized, the samples were enclosed in separate glass wiles.

3.5 Material Characterizations

The morphology of PP and flocs were identified by field-emission gun Scanning electron microscope (FEG-SEM; Carl Zeiss Sigma 500) combined with energy dispersive X-ray spectroscopy (EDS), the crystallinity of the samples were analysed by X-ray Diffraction (XRD; SmartLab SE, Smartlab Rigaku, Japan) and chemical identification of the samples from Raman spectroscopy (RAMAN; Labram HR Confocal Micro-Raman Spectrometer, Horiba, France), at Materials Characterization Facility (MCF) and DLS was analyzed on instrument Brookhaven, at Department of Physics & Materials Science (DPMS), Thapar Institute of Engineering & Technology, Patiala-147004, INDIA. The functional groups of samples were analysed using Fourier-transform infrared spectroscopy (FT-IR; Perkin Elmer – Spectrum RX-I FTIR Spectrometer) were obtained from Sophisticated Analytical Instrumentation Facility (SAIF) at Panjab University, Chandigarh. XPS data for spectra was collected from Thermofisher Nexsa XPS instrument.

Chapter 4

Results and Discussions

4.1 Electrocoagulation Results

4.1.1 Response Surface Methodology (RSM)

The EC of PP MPs using iron electrodes was investigated and modelled by CCD/RSM, using five levels of independent parameters namely, pH, current density, electrolysis time and NaCl concentration. **Table 6** illustrates the experimental design of PP electrocoagulation and results acquired with the help of Design-Expert software.

The Analysis of Variance (ANOVA) for % removal and energy consumption generated from the CCD/RSM are depicted in **Table 7 and 8** respectively. The findings of regression analysis of % removal indicate that all the four linear effects (A, B, C and D) are statistically significant (p-value ≤ 0.05). In terms of removal efficiency, raising electrolysis time and current density proved to be important for increasing PP removal. The obtained R^2 value was 0.9848 which depicts that the derived model (quadratic) can handle almost 98% of the variances and is capable of detecting the parameters within the operational ranges. Additionally, adjusted R^2 (0.9706) is in a reasonable agreement with the predicted R^2 (0.9035), further depicting the relation of experimental with the modelled data. The model has a good f-value and a very small p-value, stating its significant nature. A quadratic polynomial equation (actual equation of this model) was designed as a function of the independent parameters along with their interactions, for optimizing the response which is depicted below.

% Removal (X_1) = + 51.48162 + 0.352742 × pH + 0.350326 × current density + 0.305893 × time + 1.81875 × NaCl conc + (- 0.002362) × (pH × current density) + 0.001563 × (pH × time) + (- 0.131979) × (pH × NaCl conc) + (- 0.000087) (current density × time) + 0.029860 (current density × NaCl conc) + (- 0.012602) (time × NaCl conc) + 0.033022 × pH^2 + (- 0.002133) × $(\text{current density})^2$ + (- 0.001231) $(\text{time})^2$ + 0.080702 × $(\text{NaCl conc})^2$

The findings of regression analysis of energy consumption indicate that only three linear effects (B, C and D) are statistically significant (p-value ≤ 0.05). In terms of energy consumption too, raising electrolysis time and current density proved to be important for increasing PP removal. The obtained R^2 value was 0.9801 which depicts that the derived model (2FI) can handle almost 98% of the variances and is capable of detecting the parameters within the operational ranges. Additionally, adjusted R^2 (0.9696) is in a reasonable agreement with the predicted R^2 (0.8764),

further depicting the relation of experimental data with the modelled data. The model has a very good f-value and a very small p-value, stating its significant nature.

Table 6 Design of Experimentation for the electrocoagulation of PP MPs

Std	Run	pH	Current Density (A/m^2)	Time (min)	NaCl conc (g/L)	% Removal (X_1)	Energy consumption (X_2)
24	1	7.0	50.0	50.0	2.5	84.00	0.73
19	2	7.0	20.0	50.0	1.5	76.00	0.19
3	3	4.0	80.0	10.0	0.5	70.67	0.38
4	4	10.0	80.0	10.0	0.5	76.80	0.44
26	5	7.0	50.0	50.0	1.5	82.67	0.77
7	6	4.0	80.0	90.0	0.5	87.00	3.50
6	7	10.0	20.0	90.0	0.5	82.67	0.46
10	8	10.0	20.0	10.0	2.5	69.33	0.05
16	9	10.0	80.0	90.0	2.5	93.30	1.92
15	10	4.0	80.0	90.0	2.5	92.00	1.82
18	11	10.0	50.0	50.0	1.5	85.33	0.73
28	12	7.0	50.0	50.0	1.5	82.67	0.77
23	13	7.0	50.0	50.0	0.5	80.00	1.20
27	14	7.0	50.0	50.0	1.5	82.67	0.77
22	15	7.0	50.0	90.0	1.5	88.00	1.56
30	16	7.0	50.0	50.0	1.5	82.67	0.77
20	17	7.0	80.0	50.0	1.5	84.00	1.50
9	18	4.0	20.0	10.0	2.5	68.00	0.04
21	19	7.0	50.0	10.0	1.5	71.90	0.16
17	20	4.0	50.0	50.0	1.5	79.10	0.73
25	21	7.0	50.0	50.0	1.5	82.67	0.77
5	22	4.0	20.0	90.0	0.5	77.33	0.38
12	23	10.0	80.0	10.0	2.5	81.33	0.23
2	24	10.0	20.0	10.0	0.5	66.67	0.05
13	25	4.0	20.0	90.0	2.5	78.67	0.20
14	26	10.0	20.0	90.0	2.5	84.00	0.29
8	27	10.0	80.0	90.0	0.5	89.00	3.50
11	28	4.0	80.0	10.0	2.5	80.00	0.10
1	29	4.0	20.0	10.0	0.5	64.50	0.05
29	30	7.0	50.0	50.0	1.5	82.67	0.77

In both the recorded responses, the F-values have indicated about the order in which the independent parameters were meaningful, with electrolysis time and current density being the key parameters in the current study. The 2FI model equation was designed as a function of the independent parameters along with their interactions, for optimizing the response of energy

consumption which is depicted below. As different models were followed for the two responses, so, 2FI model equation do not contain quadratic terms.

Energy consumption (X_2) = - 0.485162 + (- 0.003196) × pH + 0.009676 × current density + 0.001933 × time + 0.309120 × NaCl conc + 0.000076 (pH × current density) + 0.000028 (pH × time) + 0.004354 (pH × NaCl conc) + 0.00440 (current density × time) + (- 0.007027) (current density × NaCl conc) + (- 0.004852) (time × NaCl conc)

Table 7 ANOVA for the % Removal of PP

% Removal (X_1)					
Source	Sum of Squares	DF	Mean Square	F Value	Prob > F
Model	1483.41	14	105.96	69.39	< 0.0001
A	53.96	1	53.96	35.34	< 0.0001
B	419.85	1	419.85	274.95	< 0.0001
C	837.32	1	837.32	548.34	< 0.0001
D	72.00	1	72.00	47.15	< 0.0001
A^2	0.2289	1	0.2289	0.1499	0.7041
B^2	9.54	1	9.54	6.25	0.0245
C^2	10.05	1	10.05	6.58	0.0215
D^2	0.0169	1	0.0169	0.0111	0.9177
AB	0.7229	1	0.7229	0.4734	0.5019
AC	0.5629	1	0.5629	0.3686	0.5528
AD	2.51	1	2.51	1.64	0.2194
BC	0.1737	1	0.1737	0.1137	0.7406
BD	12.84	1	12.84	8.41	0.0110
CD	4.07	1	4.07	2.66	0.1236
Residual	22.91	15	1.53		
Lack of Fit	22.91	10	2.29		
Pure Error	0.0000	5	0.0000		
Cor Total	1506.31	29			

A: pH, B: Current density (J, A/m^2), C: Time (t, min), D: NaCl conc (g/L)

The model adequacy was analysed through the residual analysis revealed by residual plots as the experimental data did not statistically differ from the predicted values. The residual plots have been shown in the **Fig 7**.

Table 8 ANOVA for Energy consumption during EC process

Energy consumption (X_2)					
Source	Sum of Squares	DF	Mean Square	F Value	Prob > F
Model	22.73	10	2.27	93.36	< 0.0001
A	0.0117	1	0.0117	0.4808	0.4965
B	7.60	1	7.60	312.29	< 0.0001
C	8.17	1	8.17	335.72	< 0.0001
D	1.16	1	1.16	47.83	< 0.0001
AB	0.0007	1	0.0007	0.0305	0.8632
AC	0.0002	1	0.0002	0.0072	0.9332
AD	0.0027	1	0.0027	0.1121	0.7414
BC	4.46	1	4.46	183.18	< 0.0001
BD	0.7111	1	0.7111	29.21	< 0.0001
CD	0.6026	1	0.6026	24.75	< 0.0001
Residual	0.4625	19	0.0243		
Lack of Fit	0.4625	14	0.0330		
Pure Error	0.0000	5	0.0000		
Cor Total	23.19	29			

A: pH, B: Current density (J, A/m^2), C: Time (t, min), D: NaCl conc (g/L)

(a) % Removal

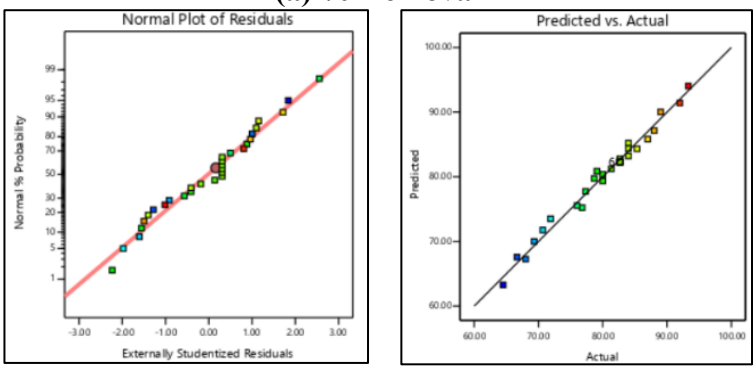

(b) Energy consumption

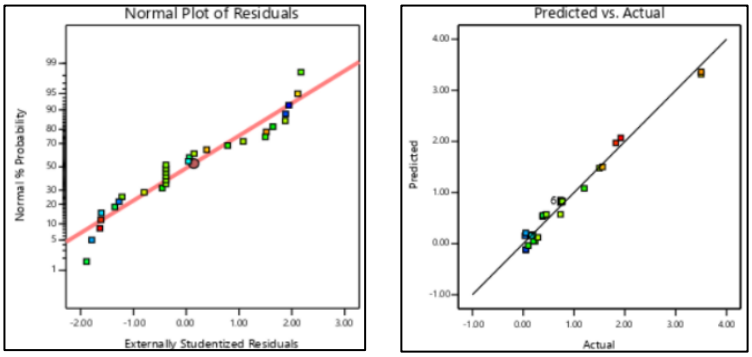

Fig 7: Residual plots and predicted vs actual plots for both responses

Table 9 Various R-squared values suggested by CCD for different responses.

Responses	R-Squared	Adj R-Squared	Pred R-Squared
% Removal (X_1)	0.9848	0.9706	0.9035
Energy consumption (X_2)	0.9801	0.9696	0.8735

Optimization was done in order to validate the model's suitability in the prediction of responses. The optimized condition with desirability factor of 0.861 was chosen and the results were summarized in the **Table 10**.

Table 10 Experimental and predicted responses values comparison at optimized condition (pH = 7, current density = 64.084 A/m^2, time = 79.076 min, NaCl conc = 2.5 g/L)

Responses	Predicted value	Experimental value
% Removal (X_1)	90.15 %	90.33 %
Energy consumption (X_2)	1.308	1.348

Fig 8 illustrates the response surface plots obtained from RSM, describing the interactive effects of current density, electrolysis time, pH and NaCl concentration on MPs removal efficiency **(a-c)** and specific energy consumption **(d-f)** during electrocoagulation using iron sacrificial electrodes.

For MPs removal, (**Figures 8(a-c)**), the results indicate that current density and electrolysis time were the most influential operating parameters. As shown in **Fig 8(a)**, removal efficiency increased significantly with increasing current density and NaCl concentration, reaching close to 89%. The enhanced performance at higher current densities can be attributed to accelerated anodic dissolution of iron, leading to the generation of larger quantities of Fe^{2+}/Fe^{3+} ions and subsequent formation of amorphous iron hydroxide flocs. These flocs promote microplastic destabilization, adsorption and sweep flocculation. Simultaneously, increasing NaCl concentration improved electrolyte conductivity, facilitating charge transfer and coagulant generation while reducing ohmic resistance. The response surface exhibited a plateau at higher operating conditions, indicating that further increases in coagulant production yielded only marginal improvements in removal efficiency.

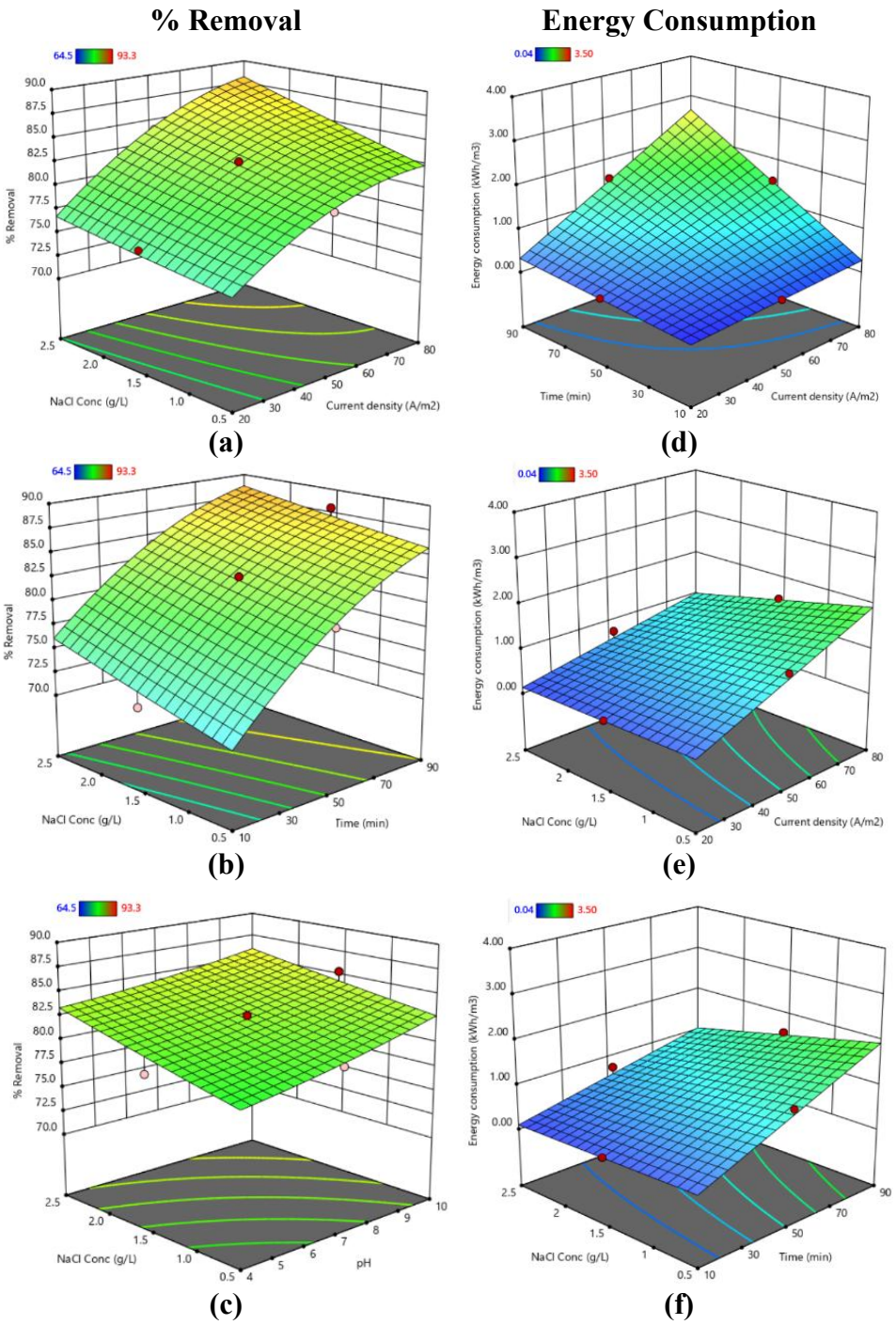

Fig 8: RSM 3-D plots for analysis of the two responses

A similar trend was observed in **Fig 8(b)**, where removal efficiency increased with increasing electrolysis time and NaCl concentration reaching up to 88%. Longer electrolysis durations promoted sustained iron dissolution and continuous production of hydroxide flocs, thereby enhancing particle aggregation and separation. However, the gradual flattening of the response surface at extended treatment times suggests that sufficient coagulant species had already been generated, resulting in diminishing returns beyond the optimum region.

In contrast, **Fig 8(c)** demonstrates that pH exerted a comparatively weaker influence on MPs removal. The relatively flat response surface indicates that efficient removal could be achieved over a broad pH range. Nevertheless, slightly higher efficiencies were obtained under near neutral to mildly alkaline conditions, which favours the formation and stability of $Fe(OH)_3$ flocs. The broad plateau region further suggests operational flexibility with respect to pH, minimizing the need for extensive pH adjustment during practical applications.

The effects of process variables on specific energy consumption are depicted in **Figures (d-f)**. as shown in **Fig 8(d)**, energy consumption increased markedly with increasing current density, reflecting greater electrical output required to sustain enhanced anodic dissolution and coagulant production. Also, it increased substantially with increasing electrolysis time due to prolonged application of electrical current reaching up to 3 kWh/m^3.

Similarly, in **Fig 8(e)**, energy consumption increased markedly with increasing current density, conversely, increasing NaCl concentration slightly reduced energy demand due to improved solution conductivity and lower cell resistance. The relatively planar surface confirms that current density was a dominant factor influencing energy consumption.

Finally, **Fig 8(f)** shows the increase of energy consumption along with the increase in electrolysis time, but higher NaCl concentrations partially offset this increase by reducing ohmic losses and decreasing cell voltage requirements. This plot indicates that electrolysis time has exerted a much stronger effect on the energy demand than electrolyte concentration.

Overall, the RSM analysis demonstrates that electrolysis time and current density are the primary factors governing both MP removal and energy consumption. Increasing these parameters enhances coagulant generation and improves removal efficiency but simultaneously increases electrical energy demand. NaCl concentration plays a beneficial dual role, improving removal efficiency while slightly reducing energy consumption through enhanced solution conductivity. In contrast, pH exhibits a comparatively minor effect on both responses, mainly influencing the formation and stability of iron hydroxide flocs rather than overall electrocoagulation performance. These findings highlight the importance of optimizing electrolysis time, current density and electrolyte concentration to achieve maximum MP removal with minimum energy consumption.

4.1.2 Artificial Neural Network (ANN) Modelling Results

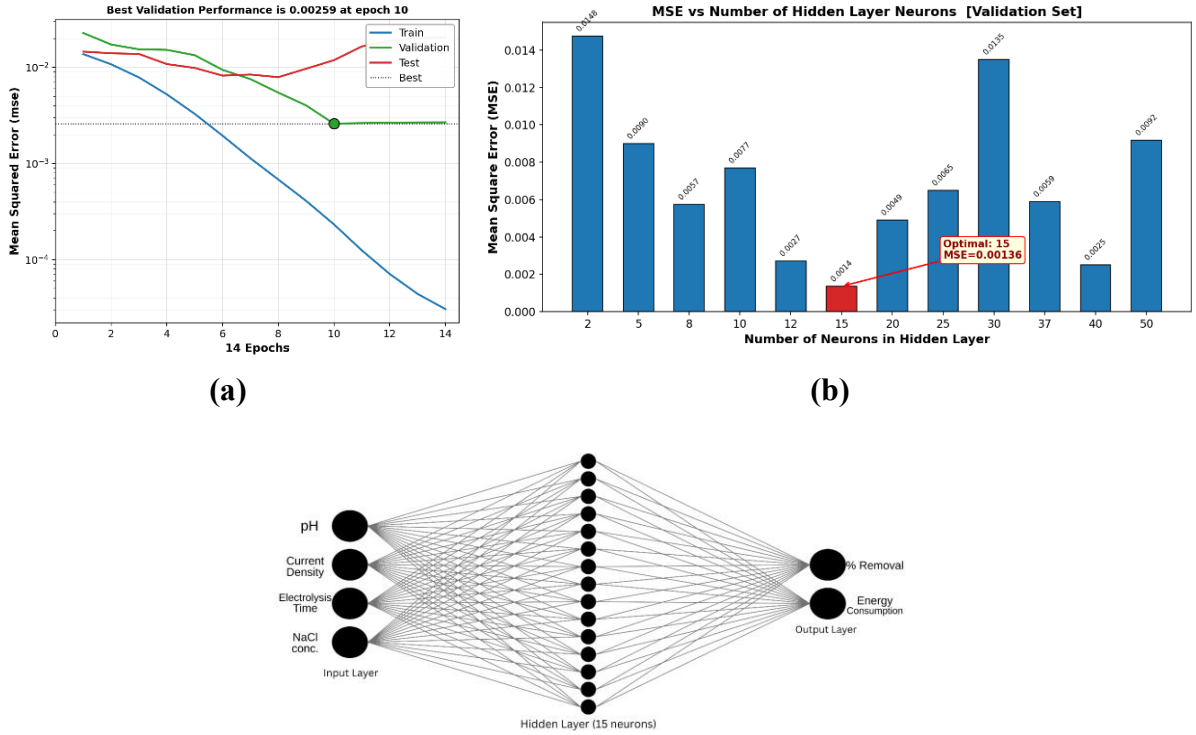

Fig 9: (a) Validation performance plot, (b) Mean Square Error vs Number of neurons in hidden layer, and (c) ANN architecture

The ANN was trained using the backpropagation algorithm to compute the gradients of loss function while Limited-memory BFGS (L-BFGS) algorithm was employed to optimize the network weights. The input and output datasets were fed into the network, and mean squared error (MSE) was used as a performance criterion. The network weights were randomly initialized, iteratively updated until convergence was achieved. **Fig 9(a)** shows ANN performance plot which signifies that validation performance was best at epoch 10 with the mean squared error of 0.00259 indicating the optimum training point. The continuous decrease in training error proves successful learning, while the stabilization of validation error and the increase in the test error after epoch 10 suggest the onset of overfitting. From **Fig 9(b)** representing the mean squared error vs hidden layer neurons, the optimized hidden layers were found to be 15 attributing to the minimum mean square error of 0.00136. The ANN architecture (4:15:2) can be observed in **Fig 9(c)**. **Fig 10** shows the regression fit of the ANN model for both the responses, % removal and energy consumption. The values of regression coefficients are close to 1, indicating a well-trained model. **Table 11** represents ANN vs RSM comparison which indicates that both models achieved R > 0.96 for both models, predicting excellent accuracy.

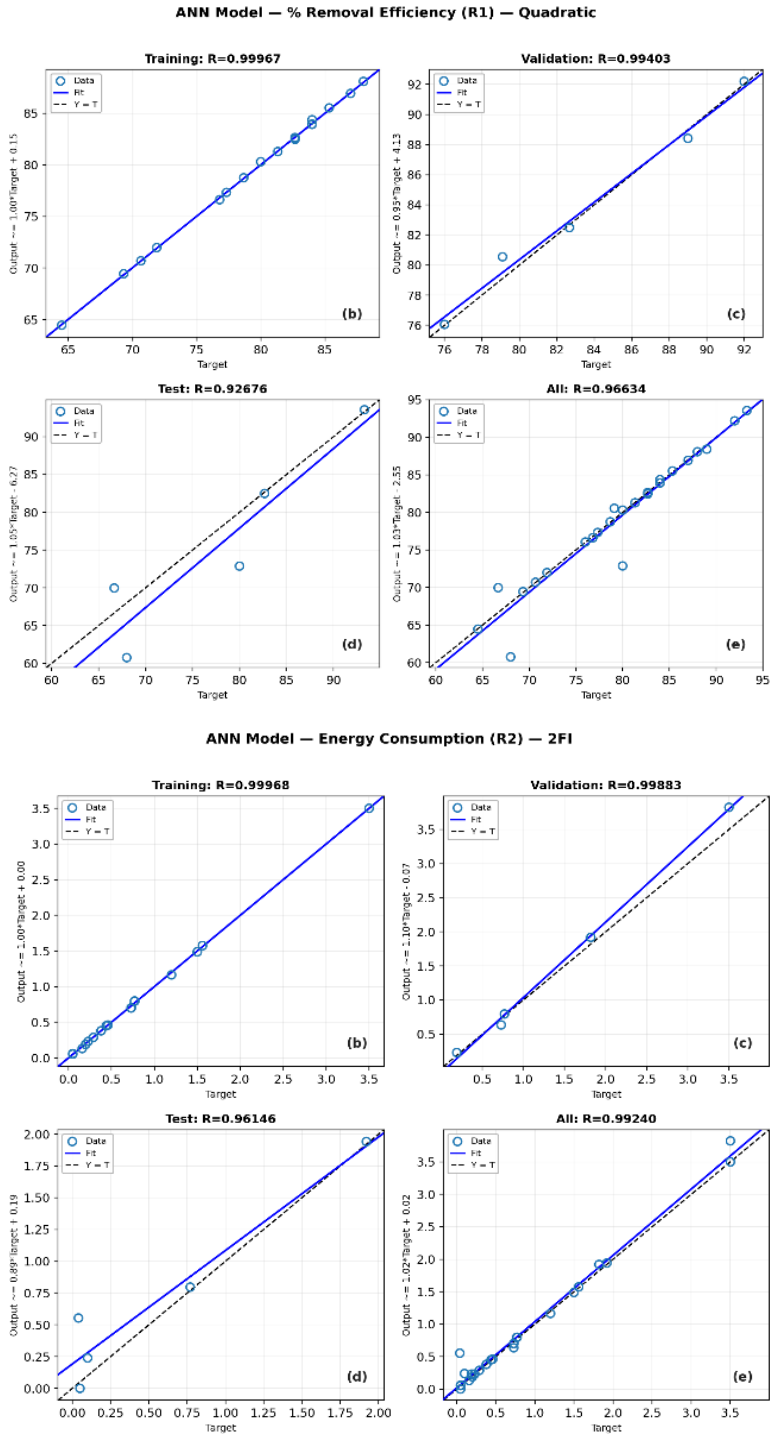

Fig 10: ANN regression plots for % Removal and Energy consumption

RSM outperforms ANN on % Removal because CCD datasets were small. Whereas, ANN performs better on Energy consumption response because ANN better captures non-linearity.

Table 11 ANN vs RSM comparison metrics

Response	Metrics	ANN (All data)	RSM	Better Model	Difference	Remarks
% Removal (X_1) (RSM: Quadratic)						
% Removal (X_1)	R	0.96634	0.99237	**RSM**	0.02603	↑ Higher = stronger correlation
	R^2	0.92216	0.98480	**RSM**	0.06264	↑ Higher = more variance explained
	MSE	3.90850	0.76330	**RSM**	3.14520	↓ Lower = less error
	RMSE	1.97699	0.87367	**RSM**	1.10332	↓ Lower = more accurate
	MAE	0.77119	0.75898	**RSM**	0.01221	↓ Lower = smaller avg error
Energy consumption (kWh/m^3) (X_2) (RSM: 2FI)						
Energy consumed (kWh/m^3) (X_2)	R	0.99240	0.99003	**ANN**	0.00237	↑ Higher = stronger correlation
	R^2	0.98189	0.98017	**ANN**	0.00172	↑ Higher = more variance explained
	MSE	0.01399	0.01532	**ANN**	0.00133	↓ Lower = less error
	RMSE	0.11827	0.12378	**ANN**	0.00551	↓ Lower = more accurate
	MAE	0.05441	0.11151	**ANN**	0.05710	↓ Lower = smaller avg error

MSE: Mean Square Error; RMSE: Root Mean Square Error; MAE: Mean Absolute Error

4.1.3 Characterization of polypropylene (PP) MPs:

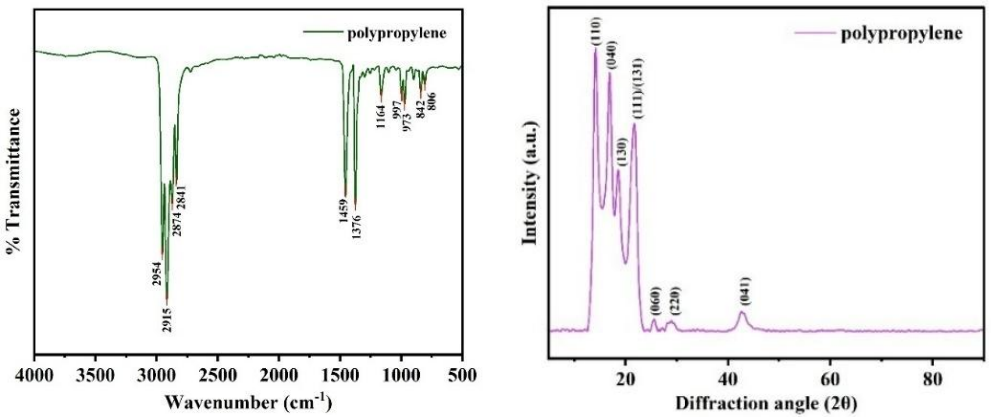

Fig 11: FTIR and XRD of Polypropylene (MPs)

Fig 11 shows FTIR spectra of PP-MPs where moderate peaks at 1376 and 1459 cm^{-1} correspond to symmetric bending vibrations of CH_3 and CH_2 respectively, while the intense peaks at 2874 and 2954 cm^{-1} are attributed to CH_3 stretching vibrations and the other one at 2915 cm^{-1} is related to asymmetric CH_2 stretching. Finally, small peaks at 806 and 842 cm^{-1} belong to C-C

stretching and CH_2 rocking vibration respectively. XRD of PP-MPs represents various intense peaks at 14.1°, 16.8°, 18.5° and 21.7°, corresponding to their crystallographic planes (110), (040), (130) and (111)/(131), respectively. Likewise, weaker reflections, at 25.5°,28.9° and 42.6°, are basically the characteristic for α-monoclinic crystalline structure of isotactic polypropylene.

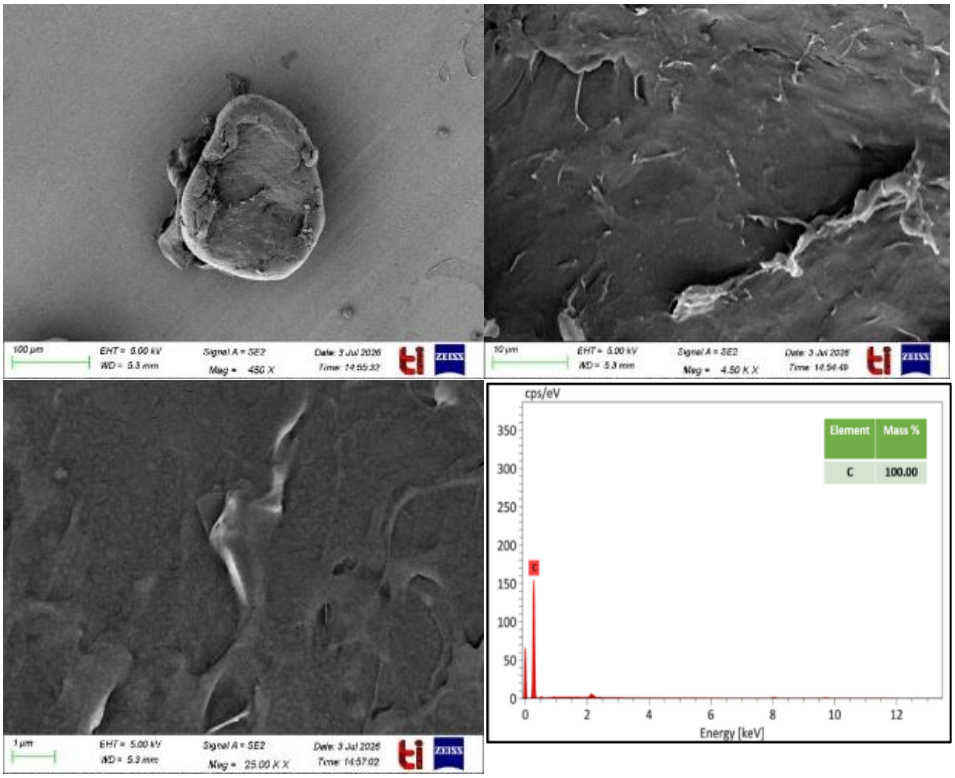

Fig 12: FE-SEM images at magnification of 100, 10 and 1µms and EDS spectra of PP

The surface morphology of PP is analysed through FE-SEM, while EDS of PP indicates the presence of carbon element before electrocoagulation **(Fig 12)**. The morphology of surface in low magnification (100 µm) is quite smooth. The 10 µm magnification reveals comparatively non-porous micro-texture of PP while, 1 µm depicts the smooth surface of pristine or non-functionalized PP.

4.1.4 Characterization results of Fe_3O_4-PP flocs:

In **Fig 13(a)**, the FTIR spectrum of Fe_3O_4-PP flocs exhibits a broad band at 3142 cm^{-1}, corresponding to O–H stretching vibrations due to surface hydroxyl groups. The adsorption bands at 2954, 2915, 2868 and 2838 cm^{-1} are attributed to the asymmetric and symmetric stretching of CH_3 and CH_2 groups, which confirms the retention of polypropylene MPs in the resultant flocs. The other characteristic PP deformation bands formed at 1456 and 1373 cm^{-1}, along with 1167, 892, 800 and 746 cm^{-1} further indicate the presence of PP in the coagulants.

The strong peak at 1018 cm^{-1} attributes to the C–O stretching vibrations, produced as a result of oxygen-rich surface functional groups. While, the most intense peaks at 557 and 457 cm^{-1} signifies the presence of Fe–O stretching vibrations, thereby, confirming the presence of Fe_3O_4 in the resultant flocs.

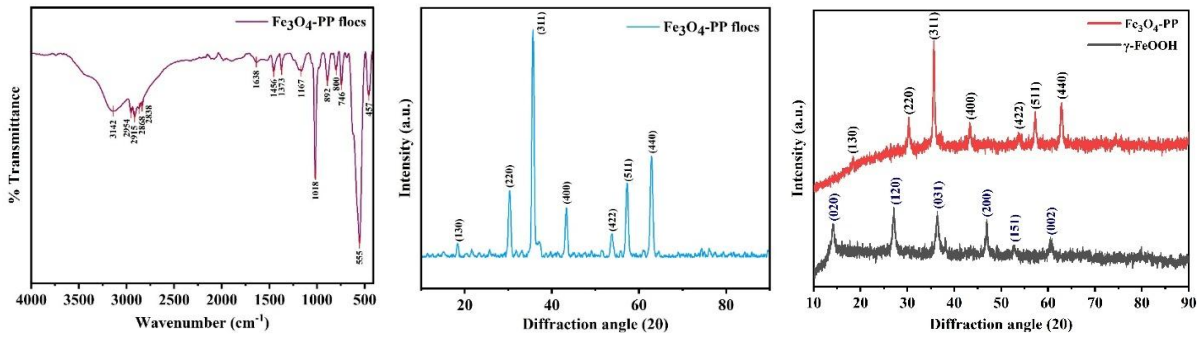

Fig 13: (a) FTIR spectra, (b) XRD spectra of Fe_3O_4-PP flocs, (c) XRD spectra representing formation of flocs during the reaction progress.

Fig 13(b) shows the XRD spectra of generated flocs giving a characteristic intense peak at 35.6, which depicts the plane 311, while other peaks at 30.3, 43.3, 53.7, 57.2 and 62.8, corresponds to planes 220, 400, 422, 511 and 440. While, one small peak at 18.3 belongs to PP and these peak values show the formation of Fe_3O_4-PP flocs.

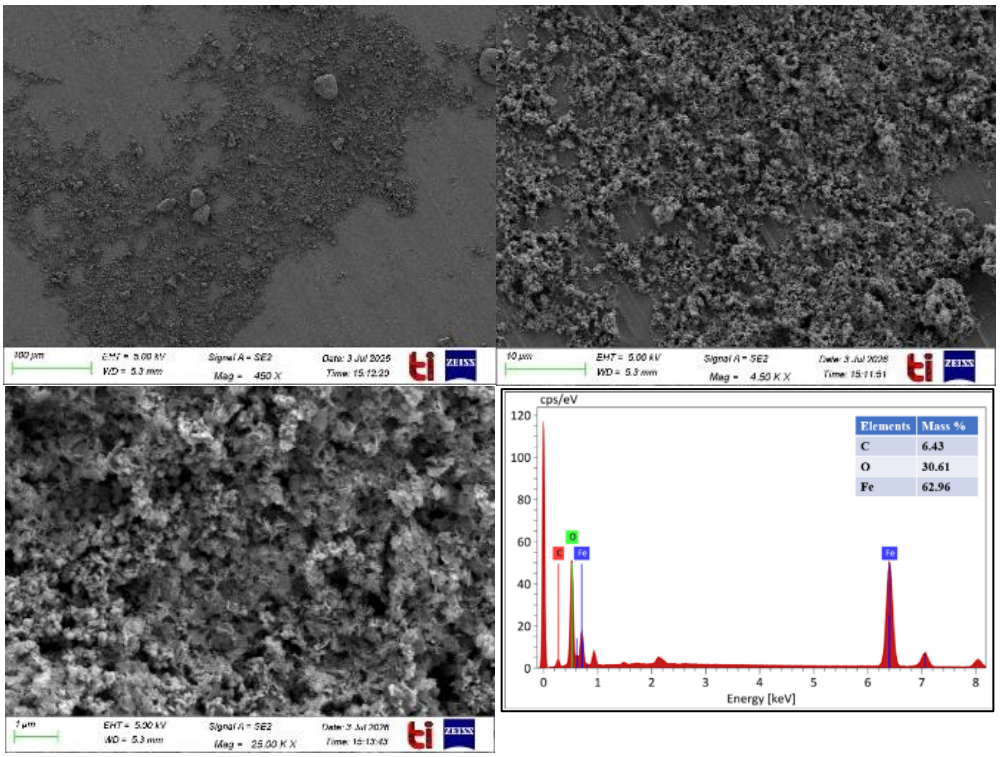

Fig 14: FE-SEM images at magnification of 100, 10 and 1µms and EDS spectra of Fe_3O_4-PP flocs

Fig 13(c) represents different flocs formation during the reaction. After analysing the data, it can be concluded that the flocs formed after 5 min of the reaction, belong to γ-FeOOH, which

is produced after continuous stirring and supply of current to ferric hydroxides flocs. These iron oxyhydroxide flocs get further converted into Fe_3O_4 after 10 min of the optimized reaction.

Fig 14 shows FE-SEM images after electrocoagulation. In 100 µm magnified image, a noticeable change from isolated pristine PP MPs to broad porous and heavily aggregated composite flocs all across the substrate is observed. While, 10 µm image shows a distinct cluster-like, rough, micro-porous network representing Fe_3O_4 particles formed during EC process have coated the PP matrix heavily. Lastly, 1 µm image proves the intricate, highly textured and grained structure containing interconnected Fe_3O_4 nanoparticles binding onto the polymer surface. EDS elemental composition shows prominent emission peaks of Fe being dominant with high mass percentage of 62.96%, while O, showing significant mass percentage of 30.61%, indicating their presence in generated flocs. Carbon (C) is also present but as a minor peak (6.43%) because it is intact.

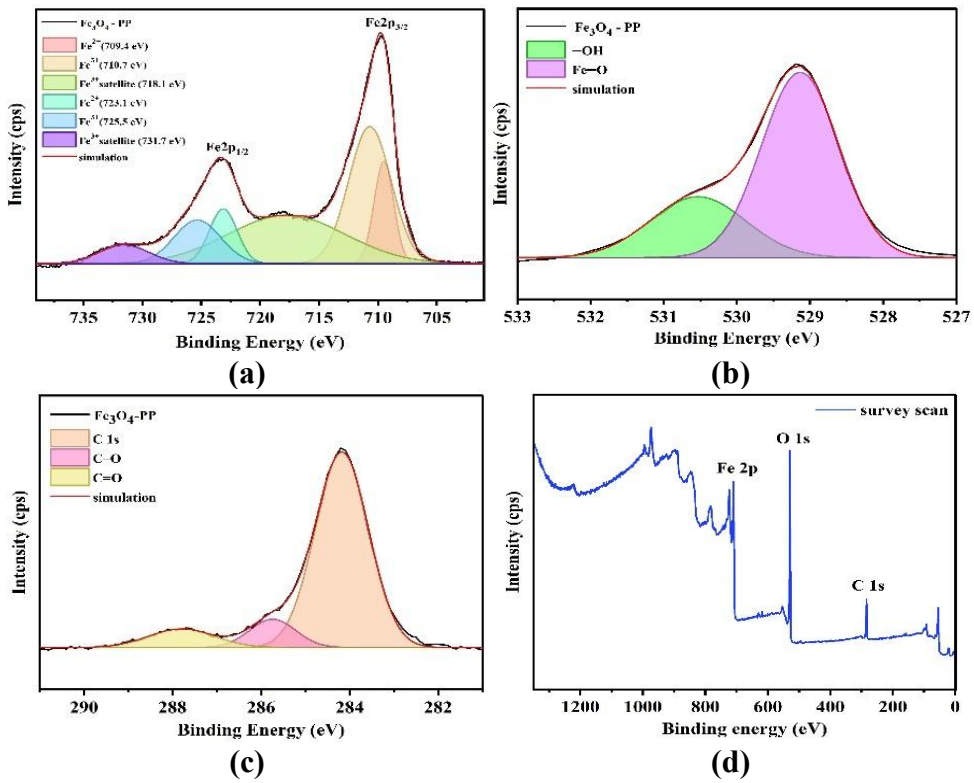

Fig 15: (a) Fe 2p spectra, (b) O 1s spectra, and (c) C 1s spectra of Fe_3O_4-PP flocs after electrocoagulation, and (d) XPS survey scan of generated flocs

X-ray photoelectron spectroscopy (XPS) was conducted to analyse the surface elemental composition and oxidation states of Fe_3O_4-PP flocs represented in **Fig 15(d)**. High-resolution deconvoluted Fe 2p spectra reveal binding energy peaks for Fe $2p_{3/2}$ and Fe $2p_{1/2}$ at 709.4 eV (for Fe^{2+}) and 710.7 eV (for Fe^{3+}), along with broad satellite peak at 718.1 eV and 731.7 eV, indicating the mixed-valence characteristic of Fe_3O_4 **(Fig 15(a))**. The deconvoluted O 1s

spectrum (**Fig 15(b)**) shows two peaks at 529.1 eV and 530.6 eV, corresponding to Fe–O lattice oxygen and surface hydroxyl groups (–OH), respectively. The C 1s spectrum (**Fig 15(c)**) depicts a dominant hydrocarbon peak at 284.1 eV which corresponds to PP matrix, along with peaks at 285.7 Ev (C–O) and 287.8 eV (C=O), indicating the interfacial entrapment of PP within Fe_3O_4 floc network. The survey scan confirms the presence of Fe, O and C on the sample surface.

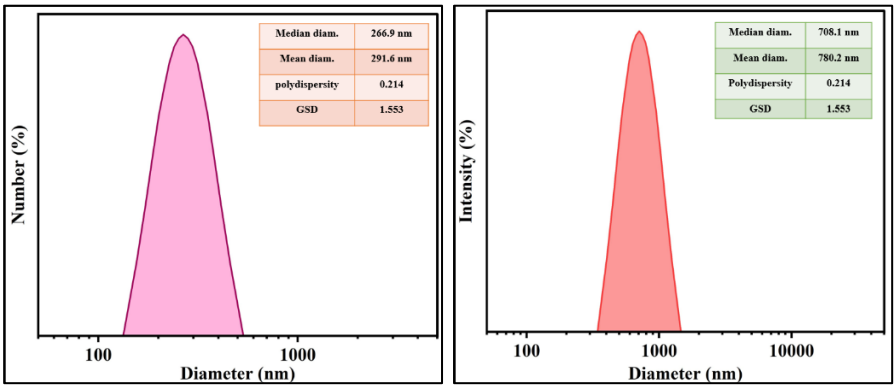

Fig 16: (a) and (b) shows number and intensity distribution of Fe_3O_4-PP flocs

DLS (Dynamic Light Scattering) was done to elucidate the hydrodynamic particle size and size distribution of Fe_3O_4-PP flocs (**Fig 16**). The number-weighted size distribution revealed the median diameter of 266.9 nm and a mean diameter of 291.6 nm. In contrast, the intensity-weighted size distribution showed a shift towards larger dimensions with a median diameter of 708.1 nm and a mean diameter of 780.2 nm, pointing to the strong dependence of light scattering intensity on particle volume. The moderate uniform floc size distribution was confirmed by the low polydispersity index of 0.214.

4.2 Carbonization results of Fe_3O_4-PP flocs:

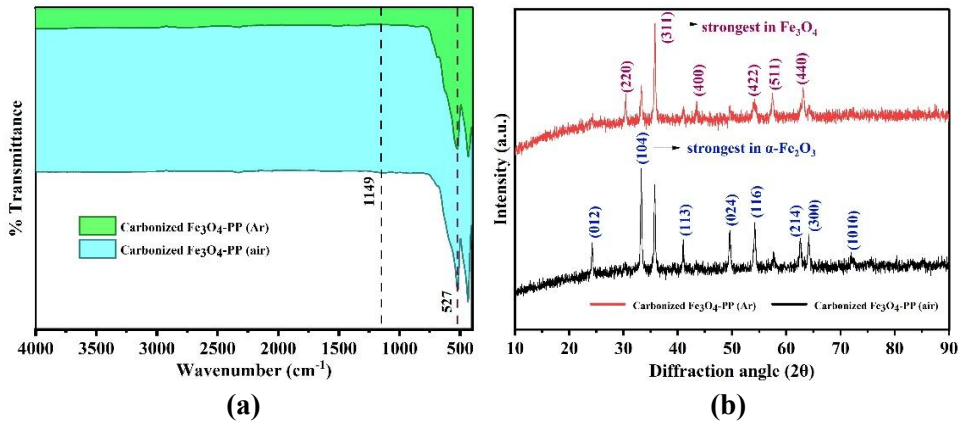

Fig 17: (a) FTIR and (b) XRD spectra of carbonized Fe_3O_4-PP flocs in air and under Ar atmosphere

Fig 17(a) compares the FTIR spectra of carbonized Fe_3O_4-PP flocs under Ar and air which indicates that high wavenumber region in both samples was virtually flat confirming the complete volatilization of organic functional groups from polymer matrix during the process, while the low wavenumber region signified few prominent characteristic peaks around 527 cm^{-1} which corresponds to Fe–O stretching vibration modes typically representing iron oxides in both the samples. Another small peak at 1149 cm^{-1} observed in carbonized Fe_3O_4-PP flocs under air showed minor surface chemical interactions formed as a result of heat treatment. **Fig 17(b)** represents XRD spectra of carbonized Fe_3O_4-PP flocs under air and Ar atmosphere. In the XRD spectra of Ar-carbonized flocs, characteristic peaks at planes (220), (311), (400), (422), (511) and (440) were observed, out of which, sharp intense peak with (311) plane is the confirmation of retention of Fe_3O_4 as the dominant phase. The reason behind its retention is the inert atmosphere, thereby, preventing the oxidation of magnetite into higher oxidation states. In contrast, the XRD spectra of air-carbonized flocs represents the intense peak with (104) plane, which is the signature reflection of hematite (α-Fe_2O_3) as the dominant phase. other characteristic peaks at planes (012), (113), (024), (116), (214), (300) and (1010). The reason behind this is that the sample was exposed to atmospheric oxygen which caused possible oxidation (phase transformation).

$$Fe_3O_4 \xrightarrow[\text{heat (air)}]{O_2} \alpha\text{-}Fe_2O_3$$

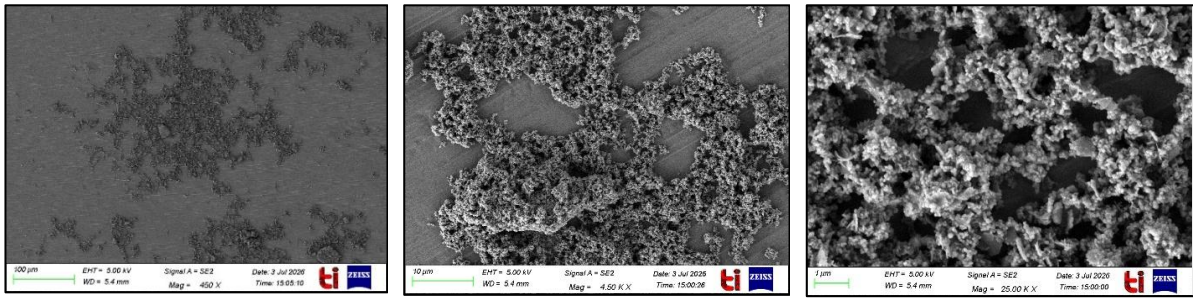

(a) **(b)** **(c)**

Fig 18: FE-SEM images at magnification of 100, 10 and 1µms carbonized Fe_3O_4-PP flocs under Ar atmosphere

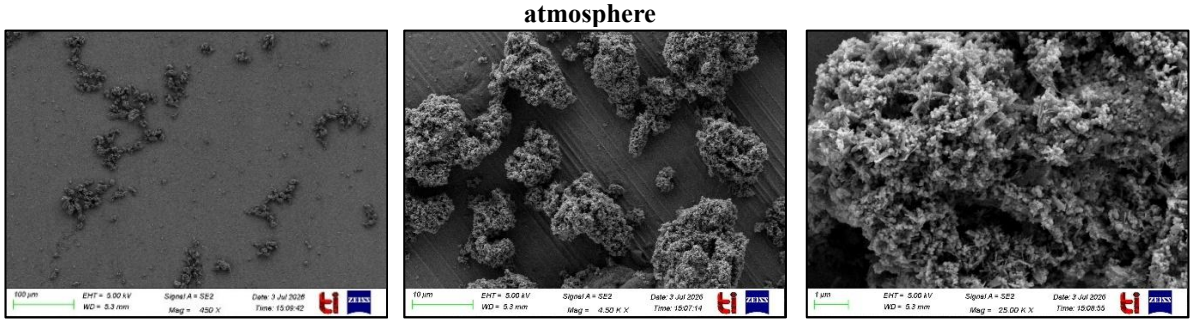

(d) **(e)** **(f)**

Fig 19: FE-SEM images at magnification of 100, 10 and 1µms carbonized Fe_3O_4-PP flocs under air

Fig 18 shows a significant morphological evolution in Fe_3O_4-PP composites upon undergoing carbonization under inert atmosphere (Ar). The images depict carbonized conductive carbon skeleton (in case of PP), along with highly textured sharp nanocrystalline grains, high 3D interconnected high network as a result of degasification and rigid, sintered Fe_3O_4-PP/carbon composite framework comprising magnetite embedded in porous carbon. At high magnification, the thermal decomposition of PP structure leads to release of volatile gaseous products creating a highly porous structure. Unlike the pre-carbonized flocs, where PP acts as a continuous amorphous coating, these post-carbonized images reveal sharp, well-defined nano-crystalline grains along an open pore network. This increase in the surface roughness and porosity enhances the active surface area, making the carbonized composite ideal for potential anode material in energy storage devices. Whereas, **Fig 19** shows Fe_3O_4-PP composites upon undergoing carbonization under air. The images depict coarser, thicker and partially collapsed pore walls, thermal sintering along with isolated, highly rigid, dense and lump-like aggregates, thereby, reducing accessible surface area and volume strain tolerance in comparison to carbonized Fe_3O_4-PP composites formed under Ar atmosphere.

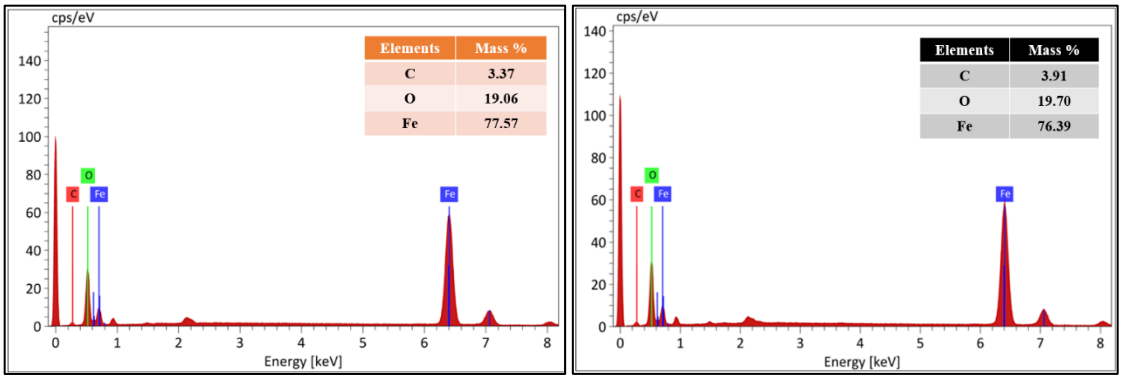

(a) **(b)**

Fig 20: EDS elemental analysis of carbonized Fe_3O_4-PP composites under (a) Ar and (b) air

Fig 20 (a) and (b) present the EDS elemental spectra and quantitative mass percentages of carbonized Fe_3O_4-PP composites under Ar and air respectively confirming the core elemental constituents as C, O and Fe. A significant rise in Fe (% weight) is observed after high temperature thermal treatment in both furnaces as carbonization caused the escape of volatile compounds. Substantial decrease in oxygen content is seen after carbonization as uncarbonized EC flocs carry significant amounts of bound moisture and hydrated iron complexes formed during water treatment, while carbon content also reduces as degradation and volatilization of hydrocarbon chains of PP occur leaving behind a thin-shelled conductive carbonaceous coating around the iron particles. Moreover, the sample carbonized in air exhibits a slightly increased

oxygen mass fraction (19.70%) and a lower Fe/O mass ratio (3.88%) as compared to sample calcined under Ar (19.06% ; Fe/O = 4.07%). This indicates the oxidation of iron species by atmospheric oxygen inside the muffle furnace, while, in tubular furnace. Oxidation is minimized and a higher metal-to-oxygen ratio is preserved.

Fig 21 shows the number and intensity- weighted graphs for both Ar- and air-carbonized Fe_3O_4-PP flocs. After comparing the DLS of both carbonized Fe_3O_4-PP flocs, it can be iterated that carbonized Fe_3O_4-PP flocs under Argon displayed larger median (302.0 nm) and mean (340.9 nm) diameter in comparison to air-carbonized sample due to the reason that controlled environment conditions i.e. inert atmosphere caused pyrolysis which resulted in promoting the cross-linking between adjacent flocs effectively causing the particles to fuse together and form larger carbon nanocomposites. Whereas, the air-carbonized flocs showed a shrinkage in their size which can be attributed to the reason that these flocs underwent thermal oxidation (volatilization) when exposed to oxygen for prolonged time causing them to lose the outer layers of flocs. As a result, this burn-off strips away the bulk volume causing the flocs to break and shrink into smaller particles (188.9 nm).

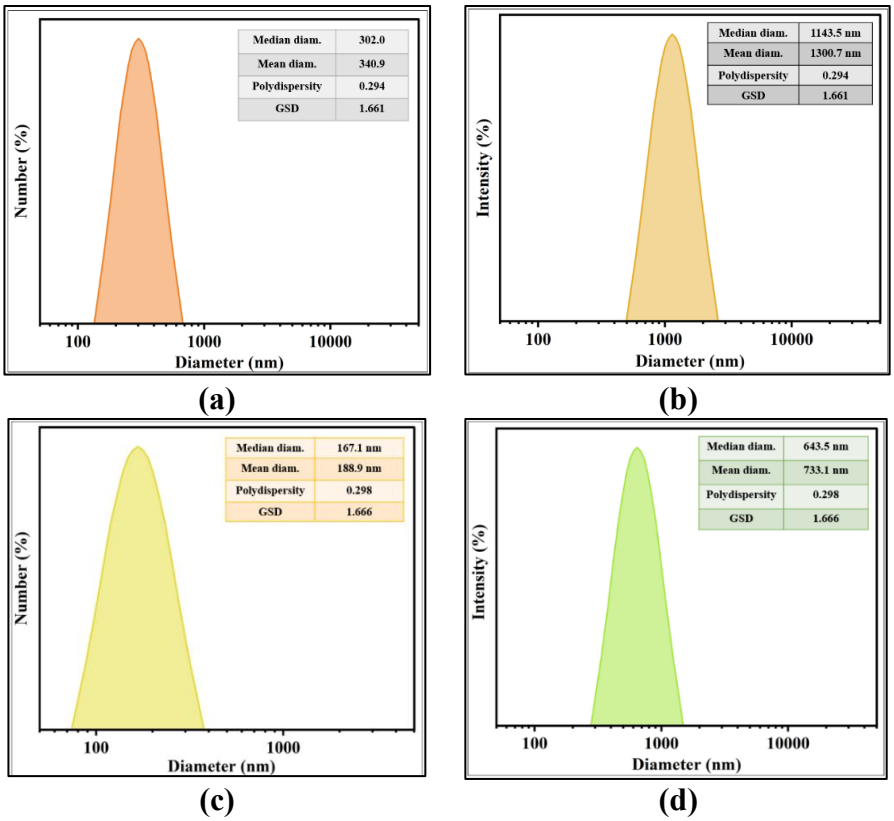

Fig 21: (a) and (b) shows number and intensity distribution of carbonized Fe_3O_4-PP flocs (Ar); (c) and (d) shows number and intensity distribution of carbonized Fe_3O_4-PP flocs (air)

XPS Fe 2p spectral analysis of carbonized Fe_3O_4-PP flocs under Ar atmosphere shows the co-existence of Fe^{2+} and Fe^{3+} components along with their Fe $2p_{3/2}$ peaks at 709.3 eV and 710.8

eV respectively. Fe $2p_{1/2}$ peaks at 723.05 eV (Fe^{2+}) and 725.2 eV (Fe^{3+}) were observed respectively. Satellite peaks at 718 eV and 731.6 eV were also seen proving the retaining of Fe_3O_4 within the carbon matrix (**Fig 22(a)**). The O 1s spectra displayed a decrease in the hydroxyl oxygen peak (530 eV) due to dihydroxylation at high temperature thermal treatment while peak (529.1 eV) due to Fe–O lattice becomes more prominent as removal of water takes place (**Fig 22(b)**). The C1s spectra shows a sharp intense peak at 284.2 eV confirms conversion of aliphatic polymer chain into a more conductive carbon network while the other peaks got reduced as compared to the before carbonization Fe_3O_4-PP flocs (**Fig 22(c)**). XPS Fe 2p spectral analysis of carbonized Fe_3O_4-PP flocs under air shows a clear distinct satellite peak at 718.3 eV which is proving that Fe^{3+} dominates in the sample kept under air in comparison to the inert environment (**Fig 23(d)**). The O 1s spectra shows a comparatively larger peak area fraction at (hump formation at 530.8 eV) as compared to tubular sample and this indicates higher surface oxidation (**Fig 23(e)**). The C 1s spectra displayed a slightly broad peak at 284.1 eV as compared to the peak shown under sample carried out in inert atmosphere (**Fig 23(f)**) which shows partial carbon oxidation**. Fig 24(g) and (h)** show survey scan of carbonized Fe_3O_4-PP flocs under Ar and air respectively. Raman spectroscopy was done to determine the phase purity and structural order and its spectra is shown in **Fig 24(i)**. In the low frequency region (800-1000 cm^{-1}), the air-carbonized sample (marked as red) showed distinct phonon modes at 224, 291, 409 and 606 cm^{-1}, characteristic of hematite (α-Fe_2O_3). Whereas, Ar-carbonized sample displayed a prominent A_{1g} vibrational mode at 661 cm^{-1} which corresponds to Fe_3O_4 crystalline phase. But, the Ar-carbonized sample showed few other peaks which indicates small oxidation as well. In the high frequency region (1200 and 1600 cm^{-1}), both carbonized samples displayed a prominent D-band peak at 1312 cm^{-1} which reflects structural disorder and edge defects within the pyrolyzed carbon matrix. The peak at 1412 cm^{-1} is assigned to amorphous carbon fragments and interfacial defect sites in the spectrum of air-carbonized sample due to partial combustion. Whereas, the peak at 1545 cm^{-1} (G-band) was exclusively visible only in Ar- carbonized sample which states that no graphitic carbon was found in air-carbonized sample. Even though G-band peak is small, but it is well preserved only in carbonized Fe_3O_4-PP flocs under Ar. These D-band and G-band provide both rapid electronic conduction pathways and abundant active sites.

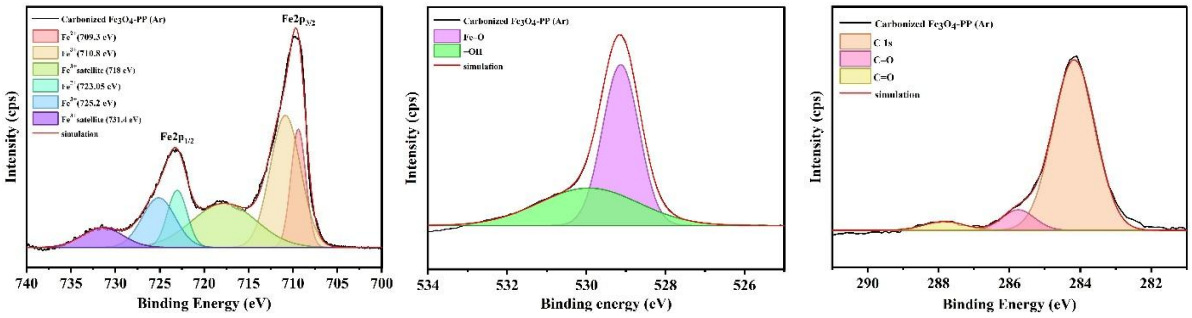

(a) (b) (c)

Fig 22: (a) Fe 2p spectra, (b) O 1s spectra and (c) C 1s spectra of carbonized Fe_3O_4-PP flocs (Ar)

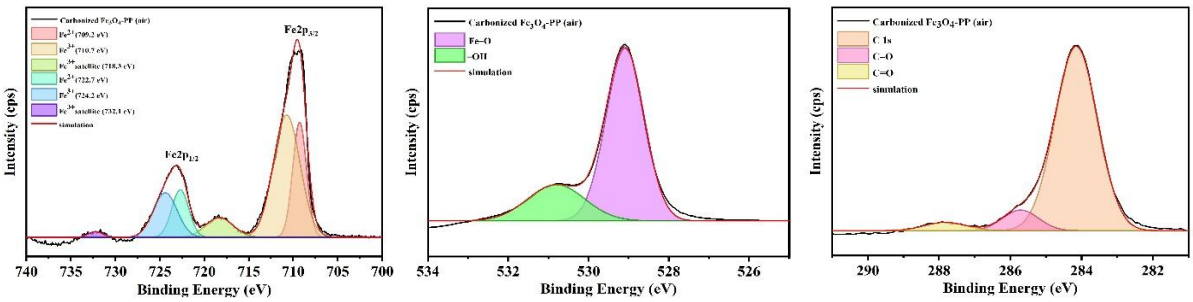

(d) (e) (f)

Fig 23: (d) Fe 2p spectra, (e) O 1s spectra and (f) C 1s spectra of carbonized Fe_3O_4-PP flocs (air)

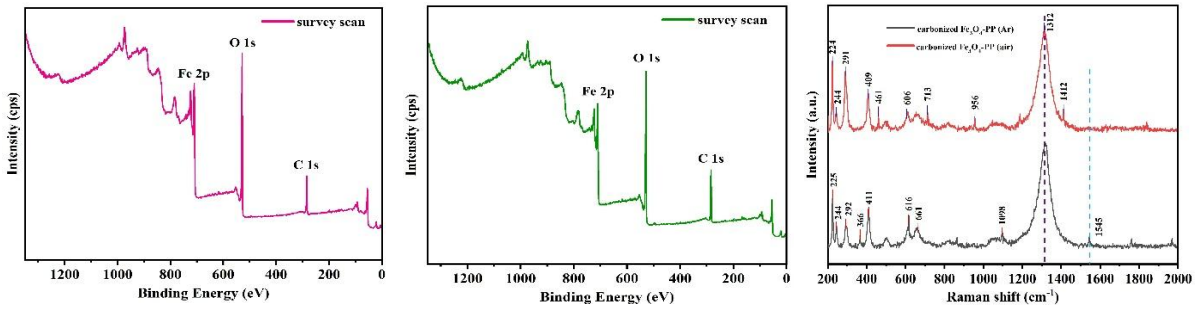

(g) (h) (i)

Fig 24: (g) XPS survey scan of carbonized Fe_3O_4-PP flocs (Ar), (h) XPS survey scan of carbonized Fe_3O_4-PP flocs (air), (i) Raman spectra of carbonized Fe_3O_4-PP flocs in air and Ar atmosphere

Potential of carbonized Fe_3O_4-PP flocs for Energy Storage Applications

Commercial Lithium-ion batteries generally use graphite as the anode material attributing to its excellent electrical conductivity, higher structural stability and lower volume expansion during cycling. However, its theoretical specific capacity is confined to 372 mAh/g. whereas, Fe_3O_4 shows very high theoretical capacity of about 924 mAh/g, making it a suitable choice over conventional anode material. nevertheless, its practical implementation alone is constricted by its poor electrical conductivity, structural instability and significant volume expansion during lithiation process. So, to address these limitations, Fe_3O_4 is generally combined conductive carbon to form Fe_3O_4/C composites. The carbon matrix increases the electrical conductivity, volume expansion and improves structural stability. Therefore, Fe_3O_4/C

composites create a balance between the high Li- storage capacity and better conductivity and mechanical stability of carbon, making them potential candidates for next-generation lithium-ion battery anodes. In the present study, the characterization results depict the successful synthesis of Fe_3O_4/PP composites with desirable properties for energy-storage applications. XRD confirmed the presence of crystalline Fe_3O_4 following carbonization, while Raman spectra showed distinct D and G bands, confirming the formation of conductive carbon. XPS verified the presence of coexistence of Fe^{2+} and Fe^{3+} species along with carbon suggesting Fe_3O_4/PP composites as their interaction promotes charge transfer and improves structural stability. A comparison of graphite, Fe_3O_4 and Fe_3O_4/PP composites is summarized in **Table 12**.

At last, the characterization results obtained in the current study indicate that the carbonized Fe_3O_4/PP composite possesses various structural and chemical characteristics which are recognized as potential for lithium-ion battery anodes, comprising a crystalline magnetite phase, conductive carbon network, defect-rich carbon core and enhanced interaction between magnetite and carbon.

Table 12 Comparison of graphite, Fe_3O_4 and Fe_3O_4/PP Composites:

Property	**Graphite**[71]	**Fe_3O_4**[72]	**Fe_3O_4/PP Composites (current work)**
Crystal structure	Layered hexagonal carbon	Cubic inverse spinel	Fe_3O_4 dispersed in carbon matrix
Electrical conductivity	Excellent	Poor	Good to excellent due to carbon network
Structural stability	Excellent	Moderate	Improved by carbon support
Particle agglomeration	Minimal	Pronounced	Suppressed by carbon matrix
Electron transport	Possible through graphitic layers	Limited by oxide conductivity	Enhanced by conductive carbon pathways
Defect density	Lower	Moderate	Higher due to carbonization, providing additional active sites
Surface area and porosity	Moderate	Moderate	Generally higher due to porous carbon
Energy storage material	Commercial anode	High-capacity candidate with stability limitations	High potential attributing to synergistic combination of conductivity and stability.

4.3 Conclusion

The present study successfully demonstrates the removal of PP MPs from water via electrocoagulation process using iron electrodes. Process optimization through RSM and ANN enabled the evaluation of effects of operating parameters on two responses i.e. MPs removal and energy consumption, providing insights about process and performance of these models. As a result of EC, generated iron oxides-rich sludge was further carbonized into Fe_3O_4/PP composites, providing a waste-valorization approach and making electrocoagulation superior and more sustainable technique over electro-oxidation and photocatalytic degradation. Further, comprehensive characterizations using XRD, Raman spectroscopy, FTIR, XPS, FE-SEM, EDS and particle-size analysis, proved successful formation of Fe_3O_4/PP composites, depicting crystalline Fe_3O_4 embedded within a carbonaceous matrix. The obtained composite exhibited desirable characteristics such as conductive carbon, a stable composite structure and coexistence of Fe^{2+}/Fe^{3+} species. Overall, this study suggests an integrated MPs remediation and value-added material generation, contributing to environmental sustainability and circular economy approach.

4.4 Future Scope

It can be suggested that future studies should focus on electrochemical measurements of the synthesized Fe_3O_4/C composites to validate its desirability for lithium-ion battery anode material. Electrochemical measurements include cyclic voltammetry (CV), Linear-scan voltammetry (LSV), Galvanic charge-discharge (GCD) and Electrochemical impedance spectroscopy (EIS) and further cycling tests should be conducted to study specific capacity, coulombic efficiency, rate capability and other required tests. Furthermore, different types of MPs and electrodes should also be investigated to evaluate the robustness and practical capability of electrocoagulation process. Finally, scaling up EC process, studying its economic feasibility and life-cycle impacts and exploring the application of Fe_3O_4/C composites in other energy storage systems, will surely increase the practical importance and sustainability of this approach.

4.5 References

(1) Birley, A. W. *Plastics Materials: Properties and Applications*; Springer Science & Business Media, 2012.

(2) Hofmann, T.; Ghoshal, S.; Tufenkji, N.; Adamowski, J. F.; Bayen, S.; Chen, Q.; Demokritou, P.; Flury, M.; Hüffer, T.; Ivleva, N. P. Plastics Can Be Used More Sustainably in Agriculture. *Commun. Earth Environ.* **2023**, *4* (1), 332.

(3) Walker, T. R.; Fequet, L. Current Trends of Unsustainable Plastic Production and Micro (Nano) Plastic Pollution. *TrAC Trends Anal. Chem.* **2023**, *160*, 116984.

(4) Gautam, B. P. S.; Qureshi, A.; Gwasikoti, A.; Kumar, V.; Gondwal, M. Global Scenario of Plastic Production, Consumption, and Waste Generation and Their Impacts on Environment and Human Health. In *Advanced strategies for biodegradation of plastic polymers*; Springer, 2024; pp 1–34.

(5) OECD. *Global Plastics Outlook: Policy Scenarios to 2060*; OECD Publishing, 2022. https://doi.org/10.1787/aa1edf33-en.

(6) Suh, W. D.; Jo, H. H.; Choi, Y.; Kim, S. Microplastics Generation from Flooring Materials under UV Exposure: A Comprehensive Analysis of Microplastics Emission and Chemical Deformation. *J. Hazard. Mater.* **2025**, *492*, 138194.

(7) Hu, K.; Yang, Y.; Zuo, J.; Tian, W.; Wang, Y.; Duan, X.; Wang, S. Emerging Microplastics in the Environment: Properties, Distributions, and Impacts. *Chemosphere* **2022**, *297*, 134118.

(8) Li, J.; Song, Y.; Cai, Y. Focus Topics on Microplastics in Soil: Analytical Methods, Occurrence, Transport, and Ecological Risks. *Environ. Pollut.* **2020**, *257*, 113570.

(9) Song, J.; Wang, C.; Li, G. Defining Primary and Secondary Microplastics: A Connotation Analysis. *Acs EsT Water* **2024**, *4* (6), 2330–2332.

(10) Zhao, K.; Wei, Y.; Dong, J.; Zhao, P.; Wang, Y.; Pan, X.; Wang, J. Separation and Characterization of Microplastic and Nanoplastic Particles in Marine Environment. *Environ. Pollut.* **2022**, *297*, 118773.

(11) Akan, O. D.; Udofia, G. E.; Okeke, E. S.; Mgbechidinma, C. L.; Okoye, C. O.; Zoclanclounon, Y. A. B.; Atakpa, E. O.; Adebanjo, O. O. Plastic Waste: Status, Degradation and Microbial Management Options for Africa. *J. Environ. Manage.* **2021**, *292*, 112758.

(12) Liu, Z.; Zhuan, Q.; Zhang, L.; Meng, L.; Fu, X.; Hou, Y. Polystyrene Microplastics Induced Female Reproductive Toxicity in Mice. *J. Hazard. Mater.* **2022**, *424*, 127629.

(13) Vickers, N. J. Animal Communication: When i'm Calling You, Will You Answer Too? *Curr. Biol.* **2017**, *27* (14), R713–R715.

(14) Lee, C.-W.; Hsu, L.-F.; Wu, I.-L.; Wang, Y.-L.; Chen, W.-C.; Liu, Y.-J.; Yang, L.-T.; Tan, C.-L.; Luo, Y.-H.; Wang, C.-C. Exposure to Polystyrene Microplastics Impairs Hippocampus-Dependent Learning and Memory in Mice. *J. Hazard. Mater.* **2022**, *430*, 128431.

(15) Casabianca, S.; Bellingeri, A.; Capellacci, S.; Sbrana, A.; Russo, T.; Corsi, I.; Penna, A. Ecological Implications beyond the Ecotoxicity of Plastic Debris on Marine Phytoplankton Assemblage Structure and Functioning. *Environ. Pollut.* **2021**, *290*, 118101.

(16) Vázquez-Rowe, I.; Ita-Nagy, D.; Kahhat, R. Microplastics in Fisheries and Aquaculture: Implications to Food Sustainability and Safety. *Curr. Opin. Green Sustain. Chem.* **2021**, *29*, 100464.

(17) Lu, Y.; Li, M.-C.; Lee, J.; Liu, C.; Mei, C. Microplastic Remediation Technologies in Water and Wastewater Treatment Processes: Current Status and Future Perspectives. *Sci. Total Environ.* **2023**, *868*, 161618.

(18) Tang, K. H. D. Remediation of Soil Contaminated with Microplastics: Strategies and Practical Implications. *Environ. Remediat.* **2026**, *1* (1), 5.
(19) Sathya, R.; Arasu, M. V.; Al-Dhabi, N. A.; Vijayaraghavan, P.; Ilavenil, S.; Rejiniemon, T. Towards Sustainable Wastewater Treatment by Biological Methods–A Challenges and Advantages of Recent Technologies. *Urban Clim.* **2023**, *47*, 101378.
(20) Su, Y.; Cheng, Z.; Hou, Y.; Lin, S.; Gao, L.; Wang, Z.; Bao, R.; Peng, L. Biodegradable and Conventional Microplastics Posed Similar Toxicity to Marine Algae Chlorella Vulgaris. *Aquat. Toxicol.* **2022**, *244*, 106097.
(21) Lozano, Y. M.; Lehnert, T.; Linck, L. T.; Lehmann, A.; Rillig, M. C. Microplastic Shape, Polymer Type, and Concentration Affect Soil Properties and Plant Biomass. *Front. Plant Sci.* **2021**, *12*, 616645.
(22) Fajardo, C.; Martín, C.; Costa, G.; Sánchez-Fortún, S.; Rodríguez, C.; de Lucas Burneo, J. J.; Nande, M.; Mengs, G.; Martín, M. Assessing the Role of Polyethylene Microplastics as a Vector for Organic Pollutants in Soil: Ecotoxicological and Molecular Approaches. *Chemosphere* **2022**, *288*, 132460.
(23) Anas, M.; Khan, I. U.; Zhang, R.-K.; Qi, S.-S.; Dai, Z.-C.; Du, D.-L. Interactive Effect of Microplastics and Fungal Pathogen Rhizoctonia Solani on Antioxidative Mechanism and Fluorescence Activity of Invasive Species Solidago Canadensis. *Plants* **2025**, *14* (13), 1972.
(24) Yang, M.; Huang, D.-Y.; Tian, Y.-B.; Zhu, Q.-H.; Zhang, Q.; Zhu, H.-H.; Xu, C. Influences of Different Source Microplastics with Different Particle Sizes and Application Rates on Soil Properties and Growth of Chinese Cabbage (Brassica Chinensis L.). *Ecotoxicol. Environ. Saf.* **2021**, *222*, 112480.
(25) Kwak, J. I.; Kim, L.; An, Y.-J. Microplastics Promote the Accumulation of Negative Fungal Groups and Cause Multigenerational Effects in Springtails. *J. Hazard. Mater.* **2024**, *466*, 133574.
(26) Dong, Y.; Bao, Q.; Gao, M.; Qiu, W.; Song, Z. A Novel Mechanism Study of Microplastic and As Co-Contamination on Indica Rice (Oryza Sativa L.). *J. Hazard. Mater.* **2022**, *421*, 126694.
(27) Harikrishnan, T.; Janardhanam, M.; Sivakumar, P.; Sivakumar, R.; Rajamanickam, K.; Raman, T.; Thangavelu, M.; Muthusamy, G.; Singaram, G. Microplastic Contamination in Commercial Fish Species in Southern Coastal Region of India. *Chemosphere* **2023**, *313*, 137486.
(28) Wu, D.; Lu, X.; Dong, L.-X.; Tian, J.; Deng, J.; Wei, L.; Wen, H.; Zhong, S.; Jiang, M. Nano Polystyrene Microplastics Could Accumulate in Nile Tilapia (Oreochromis Niloticus): Negatively Impacts on the Intestinal and Liver Health through Water Exposure. *J. Environ. Sci.* **2024**, *137*, 604–614.
(29) Zhao, Y.; Jia, H.; Deng, H.; Ge, C.; Xing, W.; Yu, H.; Li, J. Integrated Microbiota and Multi-Omics Analysis Reveal the Differential Responses of Earthworm to Conventional and Biodegradable Microplastics in Soil under Biogas Slurry Irrigation. *Sci. Total Environ.* **2024**, *907*, 168191.
(30) Meng, K.; Lwanga, E. H.; van der Zee, M.; Munhoz, D. R.; Geissen, V. Fragmentation and Depolymerization of Microplastics in the Earthworm Gut: A Potential for Microplastic Bioremediation? *J. Hazard. Mater.* **2023**, *447*, 130765.
(31) Hwang, J.; Choi, D.; Han, S.; Choi, J.; Hong, J. An Assessment of the Toxicity of Polypropylene Microplastics in Human Derived Cells. *Sci. Total Environ.* **2019**, *684*, 657–669.
(32) Rodrigo, R.; Bonastre, J.; Molina, J.; Cases, F. Electrochemical Degradation of Micro/Nanoplastics in Water: Recent Results. *J. Appl. Electrochem.* **2026**, *56* (1), 12.

(33) Kushwaha, J. P.; Singh, N. Anodic Electro-Catalytic Treatment of Polystyrene Microplastics in Water: Pathway Elucidation and Oxidative Performance. *J. Environ. Chem. Eng.* **2025**, 119017.
(34) Ma, Y.; Jin, K.; Yin, X.; Zhao, X.; Liu, Z.; Dou, Y.; Ao, T.; Li, Y.; Duan, X. Advanced Oxidation in the Treatment of Microplastics in Water: A Review. *Desalination Water Treat.* **2025**, *322*, 101135.
(35) Xiang, P.; Zhang, T.; Wu, Q.; Li, Q. Systematic Review of Degradation Processes for Microplastics: Progress and Prospects. *Sustainability* **2023**, *15* (17), 12698.
(36) Ge, J.; Zhang, Z.; Ouyang, Z.; Shang, M.; Liu, P.; Li, H.; Guo, X. Photocatalytic Degradation of (Micro) Plastics Using TiO2-Based and Other Catalysts: Properties, Influencing Factor, and Mechanism. *Environ. Res.* **2022**, *209*, 112729.
(37) Nabi, I.; Ahmad, F.; Zhang, L. Application of Titanium Dioxide for the Photocatalytic Degradation of Macro-and Micro-Plastics: A Review. *J. Environ. Chem. Eng.* **2021**, *9* (5), 105964.
(38) Silva, D. B.; Marques, A. C. TiO_2-Based Photocatalytic Degradation of Microplastics in Water: Current Status, Challenges and Future Perspectives. *J. Water Process Eng.* **2025**, *72*, 107465.
(39) Chen, G. Electrochemical Technologies in Wastewater Treatment. *Sep. Purif. Technol.* **2004**, *38* (1), 11–41.
(40) Emamjomeh, M. M.; Sivakumar, M. Review of Pollutants Removed by Electrocoagulation and Electrocoagulation/Flotation Processes. *J. Environ. Manage.* **2009**, *90* (5), 1663–1679.
(41) Mollah, M. Y. A.; Schennach, R.; Parga, J. R.; Cocke, D. L. Electrocoagulation (EC)—Science and Applications. *J. Hazard. Mater.* **2001**, *84* (1), 29–41.
(42) Geyer, R.; Jambeck, J. R.; Law, K. L. Production, Use, and Fate of All Plastics Ever Made. *Sci. Adv.* **2017**, *3* (7), e1700782.
(43) Andrady, A. L. Microplastics in the Marine Environment. *Mar. Pollut. Bull.* **2011**, *62* (8), 1596–1605.
(44) Rochman, C. M.; Hoh, E.; Kurobe, T.; Teh, S. J. Ingested Plastic Transfers Hazardous Chemicals to Fish and Induces Hepatic Stress. *Sci. Rep.* **2013**, *3* (1), 3263.
(45) Leslie, H. A.; Van Velzen, M. J.; Brandsma, S. H.; Vethaak, A. D.; Garcia-Vallejo, J. J.; Lamoree, M. H. Discovery and Quantification of Plastic Particle Pollution in Human Blood. *Environ. Int.* **2022**, *163*, 107199.
(46) Sun, J.; Dai, X.; Wang, Q.; Van Loosdrecht, M. C.; Ni, B.-J. Microplastics in Wastewater Treatment Plants: Detection, Occurrence and Removal. *Water Res.* **2019**, *152*, 21–37.
(47) Ru, J.; Huo, Y.; Yang, Y. Microbial Degradation and Valorization of Plastic Wastes. *Front. Microbiol.* **2020**, *11*, 442.
(48) Shen, M.; Song, B.; Zhou, C.; Hu, T.; Zeng, G.; Zhang, Y. Advanced Oxidation Processes for the Elimination of Microplastics from Aqueous Systems: Assessment of Efficiency, Perspectives and Limitations. *Sci. Total Environ.* **2022**, *842*, 156723.
(49) Panizza, M.; Cerisola, G. Direct and Mediated Anodic Oxidation of Organic Pollutants. *Chem. Rev.* **2009**, *109* (12), 6541–6569.
(50) Martinez-Huitle, C. A.; Ferro, S. Electrochemical Oxidation of Organic Pollutants for the Wastewater Treatment: Direct and Indirect Processes. *Chem. Soc. Rev.* **2006**, *35* (12), 1324–1340.
(51) Bharti, A.; Deb, A.; Mondal, A. Mass Transfer Driven Electro-Oxidation of Polyethylene Terephthalate Microplastics Using a Rotating Parallel Electrode System. *Polym. Degrad. Stab.* **2026**, 111990.

(52) Bharti, A.; Sengupta, S.; Mondal, A. Enhancing the Degradation of Polystyrene and Polyethylene Terephthalate Microplastics in Water Using Electrochemical Treatment at Neutral pH. *J. Environ. Manage.* **2025**, *394*, 127401.
(53) Zheng, W.; Wang, B.; Liu, Z.; Yang, H.; Chen, Z.; Sun, X. La-Doped Ti/Sb-SnO2 Electrode Enhanced Removal of Microplastics by Advanced Electrocatalysis Oxidation Process (AEOP) Strategy. *Desalination Water Treat.* **2024**, *320*, 100622.
(54) de Mello, R.; Kronka, M. S.; Rossini, E. L.; da Silva, J. C.; de Lima Gomes, P. C. F.; de Jesus Motheo, A.; Zanoni, M. V. B. Electrochemical Oxidation of Polyethylene Microplastics: From Efficient Removal to Sustainable Valorization. *J. Appl. Electrochem.* **2026**, *56* (4), 70.
(55) Mais, L.; Melis, N.; Vacca, A.; Mascia, M. Electrochemical Removal of PET and PE Microplastics for Wastewater Treatment. *Environ. Sci. Water Res. Technol.* **2024**, *10* (2), 399–407.
(56) Ning, Z.; Duan, X.; Li, Y.; Zhao, X.; Chang, L. Degradation of Polyvinyl Chloride Microplastics via Electrochemical Oxidation with a CeO2–PbO2 Anode. *J. Clean. Prod.* **2023**, *432*, 139668.
(57) Hamd, W.; Daher, E. A.; Tofa, T. S.; Dutta, J. Recent Advances in Photocatalytic Removal of Microplastics: Mechanisms, Kinetic Degradation, and Reactor Design. *Front. Mar. Sci.* **2022**, *9*, 885614.
(58) Liu, J.; Zhao, D.; Wu, X.; Wu, D.; Su, N.; Wang, Y.; Chen, F.; Fu, C.; Wang, J.; Zhang, Q. Synergistic Dual-Defect Band Engineering for Highly Efficient Photocatalytic Degradation of Microplastics via Nb-Induced Oxygen Vacancies in SnO 2 Quantum Dots. *J. Mater. Chem. A* **2025**, *13* (6), 4429–4443.
(59) Zhang, C.; Huang, L.; Nekliudov, A. Construction of Loading G-C3N4/TiO2 on Waste Cotton-Based Activated Carbon S-Scheme Heterojunction for Enhanced Photocatalytic Degradation of Microplastics: Performance, DFT Calculation and Mechanism Study. *Opt. Mater.* **2024**, *154*, 115786.
(60) Uheida, A.; Mejía, H. G.; Abdel-Rehim, M.; Hamd, W.; Dutta, J. Visible Light Photocatalytic Degradation of Polypropylene Microplastics in a Continuous Water Flow System. *J. Hazard. Mater.* **2021**, *406*, 124299.
(61) Saifuddin, M.; Ghaffari, Y.; Park, S. Y.; Kim, C. G. Rapid Surface Degradation of Co-Axially Arranged Polypropylene Globules by Nanoporous Carbonized TiO2 Assisted with UV-C. *Environ. Res.* **2022**, *212*, 113422.
(62) Chai, C.; Liang, H.; Yao, R.; Wang, F.; Song, N.; Wu, J.; Li, Y. Photocatalytic Degradation of Polyethylene and Polystyrene Microplastics by α-Fe2O3/g-C3N4. *Environ. Sci. Pollut. Res.* **2023**, *30* (58), 121702–121712.
(63) Ariza-Tarazona, M. C.; Villarreal-Chiu, J. F.; Hernández-López, J. M.; De la Rosa, J. R.; Barbieri, V.; Siligardi, C.; Cedillo-González, E. I. Microplastic Pollution Reduction by a Carbon and Nitrogen-Doped TiO2: Effect of pH and Temperature in the Photocatalytic Degradation Process. *J. Hazard. Mater.* **2020**, *395*, 122632.
(64) Liang, W.; Luo, Y.; Song, S.; Dong, X.; Yu, X. High Photocatalytic Degradation Activity of Polyethylene Containing Polyacrylamide Grafted TiO2. *Polym. Degrad. Stab.* **2013**, *98* (9), 1754–1761.
(65) Ya, V.; Martin, N.; Choo, K.-H.; Chou, Y.-H.; Lee, S.-J.; Le, N. C.; Li, C.-W. High-Pressure Electrocoagulation System with Periodic Air Replenishment for Efficient Dye Wastewater Treatment: Reaction Dynamics and Cost Evaluation. *J. Clean. Prod.* **2019**, *213*, 1127–1134.
(66) Zheng, B.; Wu, H.; Zhang, M.; Lin, S. Removal of Polystyrene Microplastics from Wastewater by Ti–Al Electrode Electrocoagulation under Pulse Current: Efficiency and Mechanism. *Water Environ. Res.* **2025**, *97* (3), e70057.

(67) Changmai, M.; Singh, M. Artificial Neural Network (ANN) and Response Surface Methodology (RSM) Algorithm-Based Improvement, Kinetics and Isotherm Studies of Electrocoagulation of Oily Wastewater. *J. Environ. Sci. Health Part A* **2022**, *57* (7), 584–592.
(68) Kothari, M. S.; Vegad, K. G.; Shah, K. A.; Hassan, A. A. An Artificial Neural Network Combined with Response Surface Methodology Approach for Modelling and Optimization of the Electro-Coagulation for Cationic Dye. *Heliyon* **2022**, *8* (1).
(69) Khanizadeh, A.; Hassanajili, S. Response Surface Methodology for Optimizing Electrocoagolation-Based Removal of Polypropylene Microplastics from Wastewater: Efficiency Comparison of Rubber and Thermoplastic-Derived Particles. *Water. Air. Soil Pollut.* **2025**, *236* (5), 299.
(70) Valdiviezo-Gonzales, L.; De-la-Torre, G.; Garcia, F. Electrocoagulation as a High-Efficiency Strategy for Microplastic Removal from Water: Process Optimization and Predictive Modeling. *Desalination Water Treat.* **2026**, 101812.
(71) Zhao, L.; Ding, B.; Qin, X.; Wang, Z.; Lv, W.; He, Y.; Yang, Q.; Kang, F. Revisiting the Roles of Natural Graphite in Ongoing Lithium-ion Batteries. *Adv. Mater.* **2022**, *34* (18), 2106704.
(72) Ren, H.; Li, H.; Barry, P.; Wang, Z.; Campos, A. R.; Takeuchi, E. S.; Marschilok, A. C.; Yan, S.; Takeuchi, K. J.; Reichmanis, E. Recent Advances in the Application of Magnetite (Fe3O4) in Lithium-Ion Batteries: Synthesis, Electrochemical Performance, and Characterization Techniques. *Chem. Mater.* **2024**, *36* (19), 9299.

Thesis

ORIGINALITY REPORT

7%	5%	4%	1%
SIMILARITY INDEX	INTERNET SOURCES	PUBLICATIONS	STUDENT PAPERS

PRIMARY SOURCES

1	Jinhee Lee, Yong-Tae Kim, Jinsub Choi. "Recycling Microplastics to Fabricate Anodes for Lithium-Ion Batteries: From Removal of Environmental Troubles via Electrocoagulation to Useful Resources", Advanced Science, 2023 Publication	1%
2	www.scribd.com Internet Source	<1%
3	journal.solusiriset.com Internet Source	<1%
4	www.frontiersin.org Internet Source	<1%
5	Submitted to Higher Education Commission Pakistan Student Paper	<1%
6	Yasir Ullah, Xingyu He, Yanqing Fang, Jun Lu. "A review about flocs in electrocoagulation process: generation, adsorption, transformation, transportation", Process Safety and Environmental Protection, 2025 Publication	<1%
7	www.ir.juit.ac.in:8080 Internet Source	<1%
8	pmc.ncbi.nlm.nih.gov Internet Source	<1%
9	pubs.rsc.org Internet Source	<1%
10	www.scilit.net Internet Source	<1%
11	Vahide Koyun, Halil Atmaca, İbrahim Küçükkara, A. Murat GİZİR. "Diode Laser-Assisted Persulfate Activation for Efficient Degradation of Pyrogallol", Springer Science and Business Media LLC, 2026 Publication	<1%
12	repository.ju.edu.et Internet Source	<1%
	www.coursehero.com	

13	Internet Source	<1 %
14	www.nsche.org Internet Source	<1 %
15	Thuy-Hanh Pham, Huu-Tuan Do, Lan-Anh Phan Thi, Pardeep Singh, Pankaj Raizada, Jeffrey Chi-Sheng Wu, Van-Huy Nguyen. "Global challenges in microplastics: From fundamental understanding to advanced degradations toward sustainable strategies", Chemosphere, 2020 Publication	<1 %
16	mspace.lib.umanitoba.ca Internet Source	<1 %
17	Azevedo, Ana Marta de Oliveira. "Sustainable and Task-Specific (Nano)GUMBOS for Chemical and Biological Analysis.", Universidade do Porto (Portugal) Publication	<1 %
18	Jerold Manuel, Ramani Kandasamy. "Bioprocess Technologies for Environmental Sustainability - Trends and Developments", CRC Press, 2026 Publication	<1 %
19	Jinling He, Kexin Li, Xianbao Xu, Yongquan Zhou, Ai Zhang, Pin Gao, Xiang Li, Gang Xue, Yanan Liu. "Beyond simple inhibition: Unveiling the non-monotonic impact and multi-level mechanisms of aged microplastics on sludge anaerobic digestion", Water Research, 2025 Publication	<1 %
20	projectshelve.com Internet Source	<1 %
21	repository.lib.ncsu.edu Internet Source	<1 %
22	repository.uantwerpen.be Internet Source	<1 %
23	worldwidescience.org Internet Source	<1 %

Exclude quotes	On	Exclude matches	< 8 words
Exclude bibliography	On		